Local comparisons of tropospheric ozone: Vertical soundings at two neighbouring stations in Southern Bavaria

Thomas Trickl[1], Martin Adelwart[2], Dina Khordakova[3], Ludwig Ries[4], Christian Rolf[3], Michael Sprenger[5], Wolfgang Steinbrecht[2] and Hannes Vogelmann[1]

[1]Karlsruher Institut für Technologie, Institut für Meteorologie und Klimaforschung (IMK-IFU), Kreuzeck-bahnstr. 19, D-82467 Garmisch-Partenkirchen, Germany

[2]Deutscher Wetterdienst, Meteorologisches Observatorium, Albin-Schwaiger-Weg 10, 82383 Hohenpeißenberg, Germany

[3]Forschungszentrum Jülich, IEK-7, Wilhelm-Johnen-Straße, 52425 Jülich, Germany

[4]Umweltbundesamt II 4.5, Plattform Zugspitze, GAW-Globalobservatorium Zugspitze-Hohenpeißenberg, Schneefernerhaus, 82475 Zugspitze, Germany

[5]Eidgenössische Technische Hochschule (ETH) Zürich, Institut für Atmosphäre und Klima, Universitätstraße 16, 8092 Zürich, Switzerland

Correspondence to: Dr. Thomas Trickl, thomas@trickl.de, Thomas-Knorr-Str. 47, D-82467 Garmisch-Partenkirchen, Germany; tel. +49-8821-50283; Dr. Hannes Vogelmann, hannes.vogelmann@kit.edu, Karlsruher Institut für Technologie, IMK-IFU, Kreuzeckbahnstr. 19, D-82467 Garmisch-Partenkirchen, Germany; tel: +49-8821-258

Abstract. In this study ozone profiles of the differential-absorption lidar at Garmisch-Partenkirchen are compared with those of ozone sondes of the Forschungszentrum Jülich and of the Meteorological Observatory Hohenpeißenberg (German Weather Service). The lidar measurements are quality assured by the highly accurate nearby in-situ ozone measurements at the Wank (1780 m a.s.l.) and Zugspitze (2962 m a.s.l.) summits and at the Global Atmosphere Watch station Schneefernerhaus (UFS, 2670 m a.s.l.), at distances of 9 km or less from the lidar. The mixing ratios of the lidar agree with those of the monitoring stations with a standard deviation (SD) of 1.5 ppb, and feature a slight positive offset of 0.6 ppb $\pm$ 0.6 ppb (SD) conforming to the known -1.8-% calibration bias of the in-situ instruments. Side-by-side soundings of the lidar and electrochemical (ECC) sonde measurements in February 2019 by a team of the Forschungszentrum Jülich shows small positive ozone offsets for the sonde with respect to the lidar and the mountain stations (0.5 to 3.4 ppb). After applying an altitude-independent bias correction to the sonde data an agreement to within just ±2.5 ppb in the troposphere was found, which we regard as the wintertime uncertainty of the lidar. We conclude that the recently published uncertainties of the lidar in the final configuration since 2012 are realistic and rather small for low to moderate ozone concentrations. Comparisons of the lidar with the Hohenpeißenberg routine measurements with Brewer-Mast sondes are more demanding because of the distance of 38 km between both sites implying significant ozone differences in some layers, particularly in summer. Our comparisons cover the three years September 2000 to August 2001, 2009 and 2018. A slight negative average offset (-3.64 ppb $\pm$ 3.72 ppb (SD)) of the sondes with respect to the lidar is found. We conclude that most Hohenpeißenberg sonde data could be improved in the troposphere by recalibration with the Zugspitze station data (1978 to 2011 summit, afterwards UFS). This would not only remove the average offset, but also greatly reduce the variability of the individual offsets. The comparison for 2009 suggests a careful partial re-evaluation of the lidar measurements between 2007 and 2011 for altitudes above 6 km where occasionally a negative bias occurred.

Key words: Tropospheric ozone, ozone sonde, ozone lidar, differential absorption

1. Introduction

The development of tropospheric ozone has been studied over more than a century (e.g., Gaudel et al., 2018; Tarasick et al., 2019). For many decades, balloon-borne ozone sondes have been a primary work horse of ozone profiling. Their measurement principle is based on the oxidation of iodide (I^-) to iodine (I_2) by ozone in a wet-chemical potassium iodide (KI) cell. Between cathode and anode of the wet-chemical cell, the oxidation reaction drives an electrical current which can be measured (two electrons per ozone molecule). Recently, nearly all stations have used the so-called ECC (electro-chemical-cell) sonde type (Komhyr 1969; 1995), featuring two cells with different potassium iodide concentrations (anode and cathode cell). Only the Hohenpeißenberg station, discussed here, still uses the older-type Brewer-Mast sondes (Brewer and Milford, 1960), which uses one cell only (with a platinum cathode and a silver anode), and a less efficient pump design (Steinbrecht et al., 1998). Ozone sondes have been characterized in numerous studies, both in flight (e.g., Attmannspacher and Dütsch, 1981; De Muer and Malcorps, 1984; Beekmann et al., 1994; Kerr et al., 1994; Jeannet et al., 2007; in recent years: Gaudel et al., 2015; Van Malderen et al., 2016; Deshler et al., 2017; Tarasick et al., 2021; Ancellet et al., 2022; Stauffer et al., 2022), and in a laboratory simulation chamber (Smit et al., 2007, 2014, 2021). Generally, the relative uncertainty of individual ECC soundings for ozone in the mid-latitude troposphere is about 5 to 10% (Logan et al., 2012; Smit et al., 2014; Tarasick et al., 2016, 2019). Following rigorous best practices, 5% accuracy can be achieved (Vömel et al., 2020; Smit et al., 2021; Tarasick et al., 2019; 2021). For Brewer-Mast soundings, the relative uncertainty in the troposphere is slightly higher, about 10 to 15% (Stübi et al., 2008; Smit et al. 2014; Tarasick et al., 2016, 2019). For tropospheric ozone from Canadian Brewer-Mast soundings prior to 1980 Tarasick et al. (2002, 2016) found a negative bias of about 20 % compared to ECC soundings.

The ozone soundings at the Meteorological Observatory Hohenpeißenberg (MOHp) of the German Weather Service (Deutscher Wetterdienst, DWD) in Southern Bavaria have been routinely carried out since November 1966, yielding one of the longest ozone-sonde time series. Brewer-Mast ozone sonde data tend to have a low bias above about 25 km altitude (Steinbrecht et al., 1998). European Brewer-Mast stations have generally used a much more extensive preparation procedure for their sondes (Claude et al. 1987), and no significant tropospheric bias has been reported for their routine Brewer-Mast soundings (de Backer et al. 1998; Stübi et al. 2008; Logan et al., 2012), as well as in chamber experiments (Smit et al., 2014).

Routine measurements with ozone sondes yield time series free of a fair-weather sampling bias. However, the balloon ascents take place at intervals of several days. Ozone profiles at short intervals (less than one minute to several minutes) can be provided by lidar sounding, but are limited to clear atmospheric conditions. Lidar measurements can generate altitude-time curtain plots and, thus, give much better insight into the impact of atmospheric transport (e.g., Browell et al., 1987; Ancellet et al., 1991; Langford et al., 1996).

At IFU (Fraunhofer-Institut für Atmosphärische Umweltforschung; now: Karlsruher Institut für Technologie, IMK-IFU) in Garmisch-Partenkirchen (Germany), a differential-absorption lidar (DIAL) with a particularly wide operating range from next to the ground up to the upper troposphere was completed in 1990 in the framework of the TESLAS (Tropospheric Environmental Studies by Laser Sounding) subproject of EUROTRAC (TESLAS, 1997; EUROTRAC, 1997, Kempfer et al., 1994). Subsequently, the system was applied for a full year (1991) within the TOR (Tropospheric Ozone Research; Kley et al., 1997) subproject of EUROTRAC (Carnuth et al., 2002). The operating range of this system was extended upwards to roughly 15 km in 1994 by introducing three-wavelength operation (Eisele et al., 1999). Due to its design, the IFU ozone DIAL features particularly low uncertainties (Trickl et al., 2020a).

82   Until 2003 the system was used for individual research projects. Between 2007 and 2018 routine measurements
83   took place, parallel to lidar measurements of water vapour (Vogelmann and Trickl, 2008) and aerosol (Trickl et
84   al., 2020b). The complementary information from these instruments has made possible a large number of
85   investigations related to atmospheric transport. The IFU ozone DIAL was recently fully described by Trickl et al.
86   (2020a).

87   The distance between MOHp and IFU is just 38 km which offers a good chance for comparisons. However, such
88   a comparison must be made with care since the atmospheric variability is high on a rather small temporal and
89   spatial scale (Vogelmann et al., 2011; 2015), mostly caused by the advection of air masses from rather different
90   source region and altitudes, with different concentrations (e.g., Stohl and Trickl, 1999; Trickl et al., 2003; Trickl
91   et al., 2011). The variability of the vertical distribution of ozone measurements rarely yields very strong
92   concentration changes, but the concentration changes are extreme for water vapour. Our lidar measurements of
93   water vapour exhibit a concentration span of more than two decades, with minima of the relative humidity (RH)
94   clearly below 1 % in layers descending from the stratosphere (Trickl et al., 2014; 2015; 2016; Klanner et al.,
95   2021).

96   Comparisons between the MOHp sonde and the IFU ozone lidar were made in the second half of the 1990s and
97   in 2001, after the first upgrading of the lidar A few of these comparisons in 1996 and 1997 were published by
98   Eisele et al. (1997; 1999). For the six cases with supposedly sufficient air-mass matching a principal agreement
99   in the free troposphere to within 5 % prevailed with occasional departures of the order of 10 %. Several
100   unpublished comparisons in 2001 showed principal agreement, but also some structural issues due to focussing
101   on stratospheric air intrusions with the STACCATO project (Stohl et al., 2003).

102   Afterwards just routine comparisons with the nearby summit stations were made. Until 2010 the lidar results
103   were compared with the long-term measurements at Wank and Zugspitze. Apart from occasional orographically
104   induced deviations an agreement mostly to within ±2 ppb was found. After these in-situ measurements ended
105   (2011) the lidar measurements were compared with the ozone measurements at the Schneefernerhaus high-
106   altitude station (Umweltforschungsstation Schneefernerhaus, UFS, 2671 m a.s.l.). UFS is located just below the
107   Zugspitze summit. Mostly a similar agreement was found.

108   However, the need for a validation of the lidar also at higher altitudes has been obvious. Such an effort became
109   more and more attractive with the growing technical performance of the system. In addition, hints on ozone
110   differences between the Zugspitze (2962 m a.s.l..) in-situ data and the MOHp values (H. E. Scheel, personal
111   communication around 2010) for 3 km a.s.l. have led to a revived interest in a thorough comparison. There have
112   been speculations about an influence of a different air composition outside the mountains at low altitudes up to a
113   few kilometres.

114   In this paper we first characterize the lidar by side-by-side ascents of ozone-sondes by a team of the
115   Forschungszentrum Jülich (FZJ). This effort, also based on the measurements at UFS, demonstrates a high
116   performance of the DIAL within the entire free troposphere, at least under winter-time conditions. Then, based
117   on this performance, we give a statistical assessment for the measurements at IFU and MOHp for the year 2018.
118   For this year we achieved the best coverage by DIAL measurements. This allows us to make an air-mass related
119   data selection to improve the comparison. Finally, we also compare lidar and MOHp sonde for two earlier
120   development phases of the lidar, for which ozone reference data at the local summit stations Wank (1780 m
121   a.s.l.) and Zugspitze exist.

122

2. Methods

2.1 Brewer-Mast sonde system at Hohenpeißenberg

MOHp (975 m a.s.l., 47.80 N, 11.00 E) is located on an isolated mountain outside the Alps, 38 km to the north of IMK-IFU and 50 km to the south-west of Munich. Brewer-Mast ozone sondes have been launched on a regular basis since November 1966. The sondes undergo a rigorous preparation procedure (Claude et al. 1987), which has remained essentially unchanged since the early 1970s. From 1995 to 2005, Vaisala RS80 radiosondes and a Vaisala PC-CORA ground station have been used in combination with the ozone sondes. This was changed to Vaisala RS92 radiosondes and DigiCora III MW31 ground equipment in 2005, to MW41 ground station in 2018, and to Vaisala RS41 radiosondes in 2019. The standard processing does not subtract a background current, but ozone sondes with non-negligible background current on the ground (corresponding to more than 2.5 ppb ozone) are not flown. The background of most sondes launched is well below this threshold. The pump temperature is assumed to be constant at 300 K, which compensates to some degree for a too weak pump correction in the stratosphere (Steinbrecht et al., 1998). The time lag is comparable to that of ECC sondes (about 20 s; see Vömel et al., 2020). A time-lag correction is not applied, but this is not critical outside regions with steep ozone gradients since the corresponding vertical shift is just of the order of 0.1 km. Each ozone profile is adjusted by multiplication with an altitude-independent correction factor (typically around 1.08, standard deviation 5 %), so that the total ozone column estimated from the sounding (including an extrapolation above approximately 30 km) matches the more accurate total ozone measurement from on-site Dobson or Brewer spectrometers, or from satellite instruments. This so-called "Dobson correction" generally improves that accuracy of the ozone sounding data in the stratosphere, but may introduce a small bias in the tropospheric data of some soundings (e.g., Stübi et al., 2008; Logan et al. 2012).

The MOHp ozone-sonde and radiosonde data are stored in the data base of the Network for the Detection of Atmospheric composition change (NDACC), from where they were imported for the study presented here.

2.2 ECC sonde system of the Forschungszentrum Jülich (FZJ)

A mobile ballon-borne sonde system of FZJ was operated at IMK-IFU (at 730 m a.s.l.), in close vicinity to the ozone DIAL (35 m), during the FIRMOS (Far Infrared Radiation Mobile Observation System) measurement campaign (Klanner et al., 2020; Palchetti et al., 2021; Di Natale, 2021; Belotti et al., 2023). Several balloons with cryogenic frostpoint hygrometers (CFH; Vömel et al., 2007; 2016), standard Vaisala RS-41-SGP radiosondes (Vaisala et al., 2019), En-Sci ECC ozone sondes (Komhyr et al., 1995; Smit et al., 2007) and COBALD backscatter sondes (Brabec, 2011) were launched. The data were transmitted to a ground station installed for this campaign at the Zugspitze summit. The combined balloon payload is well tested and regularly also used by the GCOS Reference Upper Air Network (GRUAN) (e.g., Dirksen et al., 2014).

We followed the standard operating procedures (SOP) of Smit et al. (2014) for the sonde preparation using a solution composition of 1 % and 1/10 (one-tenth) buffer for best results with sondes from the manufacturer En-Sci (Thompson et al., 2019).

For the analysis of the ECC data, the methods described by Vömel et al. (2020) are used, i.e., time lag correction and background current correction. The overall uncertainty of the ozone measurements of the ECC sondes is 5%. Due to the obstruction of the line of sight between between launch site at IMK-IFU and the ground station at the summit by the Waxenstein mountain allowed data recording only from approximately 1500 m altitude upwards. Therefore, we used the estimated ECC background current from the sonde preparation one day before a flight as

163 starting value for the background correction instead of the actual measured profile from ground up to 1500 m.

164 This results in an additional uncertainty in the lower part of the profile (2 to 3 km a.s.l.).

165 **2.4 IFU ozone DIAL system**

166 The ozone DIAL of IMK-IFU (Garmisch-Partenkirchen), located at 47.477 N, 11.064 E, and 740 m a.s.l., has

167 been developed and optimized since 1988 (Kempfer et al., 1994; Trickl et al., 2020a). It is based on a krypton

168 fluoride excimer laser, operated at 400 mJ per pulse (40 W) of narrowband radiation at 248.5 nm, two

169 Newtonian receiving telescopes (diameter of the primary mirrors: 0.13 m and 0.5 m) and 1.1-m grating

170 spectrographs for wavelength separation. Efficient stimulated Raman shifting in hydrogen and deuterium yields

171 emission at the three operating wavelengths 277.2 nm, 291.8 nm and 313.2 nm. The shorter-wave spectral

172 components are absorbed by ozone ("on" wavelengths), that at 313.2 nm ("off" or reference wavelength) is

173 almost outside the absorption region of O_3. The laser system is operated with a repetition rate of 99 Hz which

174 allows a short data-acquisition time of 41 s for the maximum number of 4096 laser shots accepted by the 24-bit

175 memory of the electronics. More shots are advisable under noisy daytime conditions in summer, but a longer

176 acquisition was prevented by laser issues.

177 The data evaluation is based on differentiating the backscatter signals, which is highly sensitive to the noise and

178 imperfections of the raw data (stored in 7.5-m bins). Therefore, the generated ozone profiles are smoothed with a

179 numerical filter. The noise fraction in the strongly decreasing backscatter signal grows with altitude. Thus, the

180 smoothing interval must be dynamically enhanced towards the tropopause (yielding a vertical resolution 0.05 to

181 0.5 km). The entire procedure is described in detail by Trickl et al. (2020a).

182 The shortwave 277.2-nm emission yields particularly accurate measurements, but the strong extinction of this

183 radiation by ozone limits the range to about 8 km. The performance in the two 277.2-nm channels is robust with

184 respect to minor misalignment, with uncertainties of about 2 to 4 ppb up to 5 km (the estimated uncertainties are

185 listed in Table 4 of Trickl et al. (2020a)). This is not the case for 291.8 nm where the optical alignment must be

186 controlled with care because of less tight focussing into the entrance slit of the far-field spectrograph. In

187 addition, the 291.2-nm backscatter signal is three times noisier than that for 277.2-nm which necessitates

188 stronger smoothing of the retrieved ozone profiles (Trickl et al., 2020a) For 5 to 8 km we specify uncertainties of

189 3 to 7 ppb. The noise of the 313.2-nm signal becomes important at large distances. As a consequence, the

190 uncertainty of the ozone mixing ratio can be become rather high in the upper troposphere and the tropopause

191 region, in particular in summer due to the stronger loss of signal caused by the higher levels of ozone.

192 Sometimes the uncertainty just below the tropopause can even exceed 10 ppb.

193 The DIAL data processing is made for different wavelength combinations (Eisele and Trickl, 2005). By

194 comparing the resulting ozone profiles an internal quality control can be achieved. The optical alignment is

195 optimized immediately after detecting an ozone mismatch in the first quicklook data evaluation. Just the laser

196 beam overlap of the different wavelength components (Trickl et al., 2020a) and the beam pointing must be

197 optimized.

198 The calibration of the ozone lidar measurements has been based from the very beginning (1991) on the accurate

199 temperature-dependent ozone absorption cross sections of the University of Reims (Daumont et al., 1992;

200 Malicet et al., 1995). These cross sections were verified for four wavelengths below 300 nm by Viallon et al.

201 (2015) to within ±0.06 %. In the presence of aerosol an aerosol correction is made with the algorithms of Eisele

202 and Trickl (2005). This correction is rather robust for the wavelength pair 277 nm - 292 nm because of the strong

203 absorption at the short "on" wavelength and the moderate wavelength difference (Völger et al., 1996).

204 Meteorological data for calculating density and temperature profiles are taken from the Munich radiosonde
205 (station 10868). The retrieved 313-nm aerosol backscatter coefficients have been routinely stored in the data
206 base of the European Aerosol Lidar Network (EARLINET) since 2007.

207 After repeated system upgrading the final performance of the lidar was reached in late 2012. In the absence of
208 aerosol the far-field ozone could be evaluated with high reliability from the 291.9-nm signal alone, after
209 precisely modelling the air number density from radiosonde data (Trickl et al., 2020). In this way the influence
210 of the daytime noise caused by the high solar background in the 313-nm reference profiles in summer could
211 frequently be avoided.

212 During the final decade of the lidar operation a fitting procedure was applied in noisy situations in the upper
213 troposphere (i.e., under high-ozone conditions in summer). This procedure reduces unrealistic curvature of ozone
214 structures caused by enhanced data smoothing, and, thus, abrupt concentration changes (in particular at the
215 tropopause) visible in the raw data are reproduced in the mixing ratio.

216 From 1991 to 2003 the DIAL was operated for focussed research projects. Routine measurements took place
217 from 2007 to 2018, until 2015 parallel to measurements with a water-vapour DIAL (Trickl et al., 2014, 2015,
218 2016, 2020b). In 2012 the highest data quality was finally reached, which included significant improvements for
219 the near-field telescope (Trickl et al., 2020a). Thus, the conditions for a meaningful system validation were
220 obtained. The operation was discontinued in February 2019, after the retirement of the first author of this paper.

221 **2.5 High-elevation surface observations**

222 Quality-assured ozone measurements at the summit stations Wank (1780 m a.s.l., 7.0 km to the north-east of
223 IMK-IFU, 47.511º N, 11.141º E) and Zugspitze (2962 m a.s.l., 8.4 km to the south-west of IMK-IFU, 47.421º N,
224 10.986º E) took place from 1978 to 2012. Since the 1990s, two or three TE 49 ozone analysers (Thermo
225 Environmental Instruments, USA) were operated simultaneously at each station. These instruments are based on
226 ultraviolet (UV) absorption at 253.65 nm. Several comparisons using transfer standards (O_3 calibrators TE 49
227 PS) were made with the World Meteorological Organization (WMO) Global Atmosphere Watch (GAW)
228 reference instrument kept at the WMO/GAW calibration centre operated by EMPA, Switzerland (Klausen et al.,
229 2003). The most recent comparison was conducted in June 2006 and confirmed that the Zugspitze O_3 data are on
230 the GAW scale.

231 Apart from the two mountain stations measurements were performed also at IFU at about 740 m a.s.l. (47.477º
232 N, 11.064º E). This laboratory was adjacent to that of the ozone DIAL.

233 At UFS (0.70 km to the south-east of Zugspitze, 47.417º, 10.980º E) ozone has been continuously measured
234 since 2002 by a team of the German Environment Agency (Umweltbundesamt, UBA) using TEI 49i instruments
235 (Thermo Electron Corporation). The gas inlet is at 2671 m a.s.l. For weekly and monthly calibration of the ozone
236 measurements a TEI 49C-PS station ozone calibrator was applied. This primary standard was annually adjusted
237 to the German ozone standard operated by UBA (UBA 204 SRP#29) that was adjusted via BIPM (Bureau
238 International des Poids et Mesures) in Paris to the NIST ozone reference standard of GAW. The measurements
239 were supported by a second instrument (Horiba APOA-370) which is equivalent to the TEI-49i. GAW
240 performance audits at the station for surface ozone took place in 2001, 2006, 2011 and 2020 (Zellweger et al.,
241 2001; 2006; 2011; 2020).

242 The uncertainty of the in-situ ozone measurements is ±0.5 ppb with respect to the WMO standard (Hearn et al.,
243 1961). This fulfills the GAW requirement.

244 The ozone data for all sites are stored at half-hour intervals. The times are specified for the end of the averaging
245 interval in Central European Time (CET, = UTC + 1 h). 1-h averages for the Zugspitze stations were made
246 available to the World Data Center and the TOAR data base (Schultz et al., 2017). In the present study we use
247 data at half-hour time resolution. The ozone series at the two Zugspitze sites have been discussed on two recent
248 scientific studies (1970 to 2020; Parrish et al., 2019; Trickl et al., 2023).

2.6 LAGRANTO Trajectories

250 Fifteen-day backward trajectories were calculated with the Lagrangian Analysis tool (LAGRANTO; Sprenger
251 and Wernli, 2015; Wernli and Davies 1997). The driving wind fields are obtained from the ERA5 reanalysis
252 dataset (Hersbach et al., 2020), which we interpolated to a 0.5º latitude/longitude grid, and on 137 vertical hybrid
253 levels. The input ERA5 data are available at a one-hour temporal resolution; the output positions of the
254 trajectories are written at 15-min time interval to allow for a more refined analysis. The start coordinates of the
255 backward trajectories are 11.064 E, 47.477 N, and the start altitudes match the altitudes of interest in the
256 soundings (see Sect. 4). The start times of the trajectories correspond to the sounding times within five minutes.
257 Finally, the start times are also shifted by several hours relative to the sounding time to assess the sensitivity of
258 the trajectory calculation on time.

3. Results

260 The main problem in comparing vertical-sounding instruments is illustrated in Fig. 1 which shows several ozone
261 measurements at Garmisch-Partenkirchen and Hohenpeißenberg in the morning of 2 October 2017. The vertical
262 distributions during that period are characterized by a descending stratospheric intrusion layer (indicated by low
263 relative humidity) of rapidly diminishing width and significant changes at all altitudes on a short time scale. This
264 reveals a considerable spatial inhomogeneity of the air mass. The approximate agreement of lidar and
265 Hohenpeißenberg ozone sonde before 6:00 CET is, thus, to some extent fortuitous although a good matching of
266 the peak ozone mixing ratio in intrusion layers at both sites is quite frequently found. Different air masses at
267 different altitudes must be assumed as indicated by matching of the sonde ozone with lidar measurements at
268 different times. The spatial and temporal requirements for comparisons can be even of the order of 1 km and 15
269 min at times (see Introduction).

3.1 Comparisons of the IFU ozone lidar and the Jülich ECC sonde

271 An optimum lidar validation became possible in early 2019. On 5 and 6 February 2019 a side-by-side instrument
272 comparison took place at Garmisch-Partenkirchen as a contribution to the FIRMOS validation project of the
273 European Space Agency. Two of the three balloons launched on 5 February were equipped with ozone sondes,
274 while both ballons on 6 February carried an ozone sonde. The ascents took place during night-time because of
275 comparisons of the CFH sondes with the water-vapour channel of the UFS Raman lidar that provides humidity
276 profiles up to at least 20 km (Klanner et al. 2021).
277 The first night of the campaign was clear. The conditions for the comparison were excellent: the sondes rose
278 almost vertically up to 8.5 km and then slowly drifted to the south-east (Innsbruck), ideal for the tropospheric
279 comparison. The balloons stayed within 20 km distance from IMK-IFU up to the tropopause (12.8 km a.s.l.) and
280 remained within 30 km up to 20 km a.s.l. The launch times of the balloons on 5 February were 18:03 CET
281 (ascent to 16.147 km), 19:03 CET (29 .475 km), and 23:00 CET (29.469 km). During the second night a cirrus
282 layer occurred in the upper troposphere which resulted in enhanced uncertainties of the DIAL data evaluation.

In Fig. 2 we present the results of the four comparisons made. The agreement between UFS and lidar is almost perfect, as known from the routine comparisons with the elevated sites between 2007 and 2018 and a number of separate comparisons (Trickl et al., 2020a). For the first three sonde ozone profiles, very small, almost altitude-independent offsets exist (0.5 to 3.4 ppb). For the fourth sonde ascent at 23:33 CET on 6 February no simultaneous lidar measurement was made. Up to 4.8 km a pronounced positive offset of the sonde ozone profile with respect to the two earlier lidar measurement (at 18:33 and 19:00 CET) is seen, but the deviation at 2.67 km is just 2 ppb if one takes the 23:30-CET measurement at UFS as the reference. We are highly content that the difference in ozone between sonde and lidar does not significantly change in the upper troposphere considering the low differential absorption for the wavelength pair 292 nm – 313 nm typically used above 6 km that implies a high sensitivity to potential technical imperfection.

In addition, we show in Fig. 2 the results of three humidity measurements with the UFS Raman lidar slightly revised with respect to Klanner et al. (2021). For comparison, we added the water-vapour mixing ratios (MRs) for the corresponding CFH sonde ascents of FZJ. The MRs indicate a high variability of the air composition on both days, up to 7 km, with several rapidly changing dry layers. The variability grows with time, as can also be concluded from the differences of Raman lidar and CFH sonde, caused by the 1-h measurement duration of the lidar needed for good stratospheric data quality. Although the vertical concentration change is much less pronounced in the ozone profiles, it is obvious that a good air-mass matching by the side-by-side ozone soundings at IMK-IFU is crucial for the quality of the comparison achieved.

As mentioned, on 6 February the quality of the lidar retrievals was deteriorated above 9 km by a layer of cirrus clouds, which required an aerosol correction. The increased level of ozone in this layer is remarkable, but is verified by the sonde. By contrast, Reichardt et al. (1996) reported full ozone depletion in a cirrus layer that we traced back to the surface of the Pacific Ocean where ozone destruction can be assumed to prevail (Kley et al., 1996). The fourth comparison shows less perfect agreement because the lidar measurements ended at 19:00 CET, hours before the last sonde ascent. This was the final measurement of the DIAL before its operation was terminated after almost three decades.

Ozone profiles are also available for the descent of the balloons. The descents took place over Northern Italy and intersected different air masses. As a consequence, strong discrepancies are seen, and we do not include these data.

From the comparison of the vertical soundings with the in-situ measurements at UFS we conclude that the ozone profiles of the lidar are slightly more quantitative than those of the sonde. The differences are rather constant as a function of the altitude. This allows us to derive uncertainties of the ozone from the DIAL measurements after subtracting the offsets of the individual sonde ascents. For quantifying the quality of the lidar measurements we took just the first three comparisons. We averaged the offset-corrected differences (Fig. 3; altitude grid 52.5 m). The averages up to 9.2 km stay within ±2.5 ppb (about ±5 %). This approximately matches the performance of the lidar at the station altitudes and now characterizes the winter-time specifications of the lidar also in the entire free troposphere after 2011. This result justifies to use the lidar as a quality standard in the comparisons with the MOHp Brewer-Mast sondes described in the following section.

The quality of the comparison shown in this section benefits from low to moderate ozone densities during the cold season, which ensures limited absorption of the laser radiation within the troposphere. In Sect. 3.2 we assess the performance for all seasons.

3.2 Comparison of MOHp ozone soundings with IFU lidar and in-situ measurements for 2018

The routine measurements with the IFU ozone DIAL since 2007 exhibit rather different annual coverages, with gaps due to system damage or upgrading periods. Starting in late 2012 the final technical performance was reached. Retrieval strategies have been further improved. The best coverage of a single year was achieved in 2018 with a total of 587 measurements and 16 (March) to 79 (September) measurements per month. Therefore, we use this year for a thorough comparison with the MOHp ozone sonde. Because of the excellent performance of the lidar verified in Sect. 3.1 we use the lidar as the reference in this comparison, together with the ozone mixing ratios from UFS.

The sonde ascents at MOHp usually take place around 6:00 CET on Monday, Wednesday and Friday, in summer just on Monday and Wednesday. We found a total of 46 of these days on which early-morning lidar measurements exist, not later than around 10:00 CET. On 36 of these days MOHp soundings are available. Thirteen of the days provided particularly good conditions with favourable temporal proximity. In the figures shown in this paper we eliminated ozone profiles for times later than 10:00 CET during a given day.

Similar to the comparisons of lidar and ECC sondes the comparisons of the lidar with the MOHp Brewer-Mast sondes reveal altitude-independent offsets of the mixing ratios. The sonde-to-sonde variations of the offsets are larger than those of the ECC sondes, consistent with the considerable uncertainties of the Brewer-Mast sondes specified by the literature (see Introduction). There is clearly an influence of layers with different ozone concentrations at both sites, but also good agreement in wide altitude ranges up to the upper troposphere after subtracting the offset. Because of this agreement it is hard to believe that the offsets are caused by systematic atmospheric differences. It is more reasonable to assume an instrumental issue as an explanation of these shifts. Furthermore, the frequently good matching of the high peak ozone in some of the stratospheric intrusion layers demonstrate the absence of concentration-dependent artefacts.

Winter

During the cold parts of the year the comparisons between the MOHp sondes and the lidar usually exhibit better quality. This is explained by less structure in the ozone vertical distributions and a wider operating range of the lidar due to the low ozone level allowing for a higher, less noisy far-field signal. We found just one example with some deviating structures of the order of ±10 ppb (10 January 2018). For the 2018 comparison we give one example in Fig. 4 (15 January). The lidar mixing ratio is of the order of 45 ppb, verified by the measurements at UFS (2660 m a.s.l.). The Brewer Mast ozone sonde shows a negative bias of 5.8 ppb relative to the lidar above 2.1 km. After removing this bias (cyan curve) the sonde ozone matches the lidar and the UFS values well for altitudes above 2.1 km. This performance almost reaches that in the examples of Sect. 3.1. Just below the tropopause there is a minor discrepancy that could be either due to the higher uncertainty of the lidar measurement at these altitudes or an air-mass difference.

For the other 2018 winter-time comparisons the constant offsets of the sondes with respect to the lidar and UFS are just +1.5 ppb to −3.0 ppb.

Summer

During the warm season the ozone distribution in the middle and upper troposphere shows structured maxima caused by long-range transport, in particular STT (stratosphere-to-tropopause transport) layers (Trickl et al., 2020b). In this altitude range a summer maximum of STT exists. Usually, these structures do not perfectly match for both sites. An example for 9 July 2018 is shown in Fig. 5.

364   Figure 5 shows good agreement in structure between the soundings at both sites up to 9 km. Again, despite the

365   pronounced ozone layering, the agreement was improved on the absolute scale by adding an altitude-independent

366   correction to the sonde values (6 ppb). The offset is usually determined up to 6 km due to the reliable

367   performance of the 277-nm-313-nm DIAL measurements, but the agreement is mostly reasonable also to higher

368   altitudes. After shifting the sonde mixing ratio we can estimate the uncertainty of the lidar measurements.

369   The elevated ozone in Fig. 5 between 3.3 km and 4.7 km can be explained by a stratospheric air intrusion, as is

370   verified by the low RH. In the upper troposphere the agreement deteriorates, but at least the increase of ozone

371   with altitude is seen in all profiles up to about 12 km. The ozone minimum around 13 km is just seen in the lidar

372   data, with just a small ozone dip in the sonde profile. It is unreasonable to ascribe this considerable discrepancy

373   to a temporary technical problem in such a limited altitude range. This example documents the difficulty of

374   quantitative comparisons of tropospheric ozone even on a horizontal scale of just 38 km.

375   In order to clarify the origin of the difference of the ozone mixing ratio in the upper troposphere we calculated

376   backward trajectories with the HYSPLIT model (http://ready.arl.noaa.gov/HYSPLIT.php; Draxler and Hess,

377   1998; Stein et al., 2015). These trajectories reveal northerly advection which implies a southward drift of the

378   sonde towards the lidar during the ascent. In the upper troposphere they did not fully explain the observations

379   within the limited maximum backward time span of 315 h for the few start altitudes selected.

380   Therefore, the trajectory calculations were extended to 350 h by using the LAGRANTO model for full-hour start

381   times between 3:00 CET and 8:00 CET, initiated at a large number of altitudes in the low-ozone range in the

382   upper troposphere. Results for start times of 7:00 CET and 8:00 CET are shown in Figs. 6 and 7. Up to a start

383   time of 4:00 CET the trajectories stayed almost completely at high altitudes. At 5:00 CET three of the

384   trajectories ended in the lower troposphere above the subtropical Pacific near a longitude of 180º, first sign of an

385   air-mass change. Later (Figs. 6 and 7) we see a clear influence of a Pacific source.

386   The low ozone level in the boundary layer above (sub)tropical oceans is well known (Eisele et al., 1999; Grant et

387   al., 2000; Trickl et al., 2003; 2010), in particular over the Pacific (Kley et al., 1996; Davies et al., 1998). In this

388   way, the lidar observations on 9 July 2018 can be understood. The launch time of the MOHp ozone sonde, 5:42

389   CET, is between the two lidar measurements. However, a delay is caused during the ascent which makes a

390   quantitative understanding difficult.

391   The moderate sonde RH above 12.3 km indicates a potential admixture of aged stratospheric air in this altitude

392   range above MOHp, which would explain the high ozone mixing ratios of more than 120 ppb.

393   Figures 5 and 8 show a rather constant negative ozone offset of the sonde profiles. The ozone profiles can be

394   brought into much better agreement with the lidar and UFS by upward shifts of 6 ppb and 10 ppb, respectively.

395   In Fig. 9 one sees one of the very rare cases of an ozone mismatch between sonde and lidar up to elevations

396   clearly above the mountain sites (1 km above the Zugspitze summit). We did not shift the MOHp profile (e.g.,

397   by 3 ppb) to reduce the mismatch since this would deteriorate the agreement above 4 km.

398   *Offsets*

399   The offsets of the MOHp data from the DIAL profiles were evaluated for all 36 comparison days. The result of

400   the statistical assessment is displayed in Fig. 10 where also the differences between the lidar results for 2671 m

401   a.s.l. and the GAW measurements at UFS are shown. Just one case was eliminated in the comparison of lidar and

402   UFS: A strong negative shift of −7 ppb can be seen in Fig. 5 where UFS is located in the falling edge of a high-

403   ozone range.

404 As found for the lidar measurements over many years (examples: Trickl et al., 2014, 2015, 2016, 2020b) the
405 lidar ozone agrees with that at UFS to within ±3 ppb (mostly ±2 ppb). The agreement would perhaps be better if
406 orographic vertical displacements and air flows on the ozone profiles would be considered (Carnuth et al., 2000;
407 2002; Yuan et al., 2019; Trickl et al., 2020a). The average difference between lidar and UFS for 2018 (blue
408 horizontal line in Fig. 10) is 0.736 ppb ± 1.46 ppb (standard deviation). A positive offset had also been found for
409 an earlier four-day comparison with the Zugspitze summit, but with even higher uncertainty (Trickl et al.,
410 2020a). A positive offset of this size could be expected from the highly accurate cross-section measurements of
411 Viallon et al. (2015), who determined a negative bias of 1.8 % of in-situ ozone data calibrated with the WMO
412 standard. This relative difference becomes more important on the absolute scale in summer than in winter
413 because of the higher ozone values. However, the statistical noise of the differences is too high to allow
414 resolving such an effect.

415 The offsets between the MOHp sonde and the lidar, again preferentially determined in the range up to 6 km, are
416 substantially higher than those between the lidar and UFS (red filled squares in Fig. 10). The offsets of the ozone
417 sondes range from −12 ppb to +4 ppb, with an average of −3.77 ppb (red horizontal line in Fig. 10) and a
418 standard deviation of 4.22 ppb.

419 We exclude the lowest altitudes from the comparison where obvious differences in ozone exist, e.g., due to local
420 night-time ozone depletion effects. It is important to note that just in seven cases of the 36 comparisons for 2018
421 lower ozone in the sonde profiles reached up to more than 2.67 km (UFS), in three cases to more than 3 km
422 (Zugspitze summit). We conclude that differences between the Zugspitze sites and the MOHp sonde are mostly
423 related to sonde calibration issues and not to differences in air-composition as suspected earlier.

424 ***Differences***

425 In order to determine the quality of the lidar measurements within the free troposphere we show in the three
426 panels of Fig. 11 average differences between lidar and offset-corrected MOHp sonde data as a function of
427 altitude and for three different ozone conditions, roughly below 50 ppb (low ozone; top panel), between 50 to 70
428 ppb (moderate ozone; second panel) and more than 70 ppb (high ozone; bottom panel), respectively. On a given
429 day, the lidar ozone profiles agreeing best with the MOHp profile was taken. We also give the percentages of the
430 averages with respect to the offset-corrected sonde ozone. At high altitudes the sonde ozone is a more useful
431 reference than the lidar in the case of high ozone because of the considerable absolute uncertainty caused by the
432 loss of laser radiation by absorption in ozone.

433 For winter-type conditions (top panel) the six examples averaged do not exhibit a significant vertical ozone
434 structure which made the analysis straight forward and yields small average differences between ±1 ppb and ±3
435 ppb, in agreement with the conclusions in Sect. 3.1. For moderate ozone (second panel) and high ozone (bottom
436 panel), mostly during the warm season, the vertical distributions are more complex with changes on a time scale
437 of even less than one hour. Here, we eliminated the data for a few pronounced ozone peaks and dips that differed
438 at both stations. The six high-ozone cases were restricted to July and August.

439 The averaged distributions of the differences exhibit oscillations. These oscillations were analysed for coherency
440 (not shown), but no systematic behaviour was identified. Thus, we ascribe the structure to noise. The noise
441 contains both an atmospheric and an instrumental component.

442 Beyond the days and years of the comparison there are occasionally extreme cases with 100 to 150 ppb in the
443 middle and upper troposphere. This can lead to lidar uncertainties even up to more than 20 ppb during daytime,
444 also because the raw signal becomes comparable with the additional solar background noise. In the most severe

445 cases the stratospheric ozone rise cannot be seen in the lidar data during daytime, and the ozone profile is cut off

446 in the upper troposphere for archiving.

447 The analyses for 2018 do not reveal significant systematic differences between the lidar values and the offset-

448 corrected sonde data in the entire free troposphere (based on the numbers underlying Fig. 10). This confirms the

449 conclusion in Sect. 3.1 for the quality of the lidar, now for all seasons. The maximum noise excursions can be

450 interpreted as maximum combined uncertainties of lidar and corrected sonde in a given altitude range (slightly

451 overestimated due atmospheric differences in ozone between both sites). The results of this analysis confirm the

452 estimates in Table 4 of Trickl et al. (2020a).

3.3 Comparisons of MOHp sonde, IFU lidar and in-situ measurements at summits in 2009

453

454 The results in Sect. 3.2 suggested to look also at a few earlier years. We select 2009 from the period of routine

455 measurements as another year of comparison. The lidar raw data were noisier than for the period after 2012 and

456 a tiny electronic ringing effect had to be removed mathematically. Thus, the uncertainties of the ozone profiles

457 above 6 km are higher than after the final system upgrading in 2012, particularly in summer. As a consequence,

458 a lidar validation is desirable at least for the upper troposphere. More importantly, in 2009 high-quality ozone

459 data still exist for the summit stations Wank (1780 m a.s.l.) and Zugspitze (2962 m a.s.l). These stations benefit

460 from more frequent direct advection compared with UFS.

461 In 2009 the lidar was operated just until October which, nevertheless, allows us to make a reasonable number of

462 comparisons with MOHp. The lidar operation was stopped afterwards since there were more and more cases of

463 single-bit errors in channel 5 of the transient digitizer system which had to be sent for repair. These errors

464 induced unrealistic data in the upper troposphere.

465 We identified a total of 23 days suitable for comparisons. On just eight of these days lidar measurements were

466 made in optimum temporal proximity. We find more deviations in the profiles than for 2018. In part, this can be

467 explained by atmospheric variability and insufficient air-mass matching. In addition, as mentioned, the raw data

468 of the lidar are noisier and some weak ringing had to be removed. This caused elevated uncertainties above 6

469 km. Nevertheless, the data allowed us to determine offsets for the MOHp ozone profiles, after verifying the data

470 quality of the lidar with the Zugspitze and Wank in-situ ozone.

471 In Fig. 12 we show the results of the analysis for 2009. The difference between IFU DIAL and Zugspitze is

472 −0.165 ppb ± 1.36 ppb (standard deviation), between DIAL and Wank +0.714 ppb ± 1.20 ppb. The DIAL ozone

473 below the Wank altitude is increasingly uncertain because of alignment issues of the near-field telescope.

474 In an earlier comparison for May 1999 (Trickl et al., 2020a) we selected a lower altitude in the DIAL data (2786

475 m) and found better agreement with the Zugspitze data, but, still, a slight positive offset with respect to the

476 station. This is not attempted here, although we can see the effect of orographic lifting in some examples.

477 For 2009 the offsets between DIAL and MOHp sondes were determined primarily by between 2 and 5 km. The

478 sonde offset obtained in this way is, again, negative on average (−1.500 ppb), with a standard deviation of 2.67

479 ppb, both being are less pronounced than in 2018.

480 Figure 13 shows a comparison on 12 January 2009, demonstrating excellent agreement between both systems

481 after offset correction, except for the upper troposphere and lower stratosphere. In this case, the first lidar

482 measurement took place at 9:20 CET, i.e., substantially later than the sonde ascent. Thus, the comparison has its

483 limits. In the morning of 12 January westerly advection was revealed by HYSPLIT backward trajectories above

484 at 7 km a.s.l. This air mass originated below 2 km over the subtropical Atlantic. This could explain the slightly

485 lower ozone level around this altitude in the lidar results.

486 Another interesting example is August 17 (Fig. 14). The agreement between lidar and ozone sonde is highly
487 satisfactory up to 5.4 km and quite reasonable up to 10 km. However, between 10 km and 14.5 km the lidar
488 ozone is extremely low, in contrast to the sonde data. The pronounced ozone increase in the sonde data above 10
489 km is difficult to explain since the elevated RH values suggest neither a low tropopause nor the presence of a
490 stratospheric intrusion that typically features RH values of a few per cent at most (Trickl et al., 2014; 2015;
491 2016). On the other hand, the ozone peak above IMK-IFU descending roughly from 10 to 8 km is attributed by
492 HYSPLIT calculations to subsiding air, indicating the presence of an intrusion layer. It is interesting that the
493 rather short delay of the lidar measurements (7:00 CET to 9:15 CET) with respect to the sonde ascent (launch
494 time 5:57 CET) can result in such a considerable difference.

495 Again, 350-h LAGRANTO trajectories were calculated for start times above IMK-IFU between 3:00 CET and
496 8:00 CET (interval: 1 h) and start altitudes within the low-ozone layer. Until 6:00 CET the influence of marine
497 boundary layers is almost absent. Afterwards, the trajectories reveal a growing import from the first 600 m above
498 the subtropical Atlantic Ocean. In Fig. 15 the LAGRANTO results for 8:00 CET are shown.

499 In some cases the lidar seems to exhibit a negative bias with respect to the sondes in the upper troposphere. It is
500 advisable to re-examine a major part of the data between 2007 and 2011, also including strategies developed
501 later. For example, an exponential decay of the analogue signal was identified with the much lower noise of the
502 final setup (Trickl et al., 2020a) which must be addressed.

3.4 Comparisons of MOHp sonde, IFU lidar and in-situ measurements summits in 2000 and 2001

504 The period September 2000 to August 2001 is suitable for another comparison when a large number of STT-
505 related measurement series were made as a contribution to the STACCATO project (Stohl et al., 2003;
506 examples: Trickl et al., 2003; 2010; 2011; Zanis et al., 2003). These measurements were made with the noisier
507 detection electronics of Eisele et al. (1999), but had the advantage that single-photon counting was used for the
508 "solar blind" "on" detection channels which added linearity above 5 km (starting in spring 1997). The counting
509 system could no longer be computer controlled after 2006. A new one was installed after highly positive results
510 in other IFU lidar systems (Klanner et al., 2021) in autumn 2018, too late for this comparison effort.

511 The focus on STT during the STACCATO period made the comparisons a challenge because of the pronounced
512 layering. However, on 11 of the useful 20 days of comparison there was reasonable temporal proximity, due to
513 running long time series. The agreement between the lidar and the MOHp sonde was much better than expected
514 in the entire free troposphere. The agreement (after offset-correcting the MOHp profiles) is almost perfect during
515 the cold season. But also under high-ozone conditions the comparisons do not reveal systematic differences
516 beyond the sonde offsets.

517 Two examples for elevated ozone are shown in Figs. 16 and 17. The good comparisons support our earlier work
518 (Trickl et al., 2003, 2010), and we tend to ascribe this to the satisfactory performance of the single-photon
519 counting system.

520 For several weeks a strange ozone rise towards the ground was observed in the lidar data below 1.5 km. This
521 effect disappeared after realigning the near-field telescope and the normal early-morning ozone drop returned.

522 However, the offsets of the MOHp mixing ratios necessary to achieve good agreement are, again, quite
523 substantial (Fig. 18). Due to the larger system noise during that period also the differences between lidar and the
524 stations are higher than those in the preceding sections, and comparable with those of the mentioned four-day
525 comparison for May 1999 (Trickl et al., 2020a). The statistical analysis yields the following average differences
526 and standard deviations:

13

527   IFU DIAL – Zugspitze: 1.22 ppb ± 1.81 ppb

528   IFU DIAL – Wank   −0.15 ppb ± 2.26 ppb

529   MOHp – IFU DIAL   −5.88 ppb ± 3.35 ppb

530 **4. Discussion and Conclusions**

531 For some time tropospheric differential-absorption ozone lidar systems had a bad reputation: The method is
532 highly sensitive to imperfections in the signal acquisition since the ozone number density is obtained by
533 differentiating the backscatter signals (Trickl et al., 2020a). In addition, a lidar covering the entire troposphere
534 and the lowermost stratosphere features a dynamic range of the backscatter signal of about eight decades, which
535 means an extreme challenge for the detection electronics.

536 Based on continual improvements, starting with the 1994 system upgrading, the IFU ozone DIAL gradually
537 approached a high performance until 2012, but minor potential for improvements remains. Comparison with the
538 nearby mountain stations quite early demonstrated an uncertainty level of ±3 ppb in the lower troposphere.
539 Occasional comparisons with ozone sondes launched at the Hohenpeißenberg (1996 to 2001, distance 38 km)
540 were rather satisfactory up to the tropopause region.

541 Here, we analyse the lidar performance in three periods during its technical development in a more
542 comprehensive manner. The best agreement was found for the side-by-side comparison with balloon ascents of
543 ECC ozone sondes performed by the FZJ team at IMK-IFU in February 2019. Just small, altitude-independent
544 offsets had to be subtracted from the sonde data to achieve agreement. The lidar itself agreed with the three local
545 summit stations. For all three years and all stations we determined a positive bias of the lidar of just 0.6 ppb ±
546 0.6 ppb (standard deviation). This value seems to reflect the -1.8-% calibration deficit of the WMO calibration of
547 the in-situ ozone data. Thus, the lidar could be even free of bias in the lower free troposphere, reflecting the high
548 quality of the calibration source (Sect. 2.4).

549 For the more distant MOHp sonde the comparisons are more complex because of the high atmospheric
550 variability (Vogelmann et al., 2011; 2015). This variability is particularly severe in summer when the
551 atmospheric layering is more pronounced. Nevertheless, there was enough agreement in certain altitude ranges
552 for examining the reliability of the ozone profiles obtained from the DIAL, also before the final modifications in
553 2012. Between 2007 and 2011 we suspect an occasional slight negative summertime bias of the lidar of the order
554 of 5 ppb above 6 km. This could be due to interfering structures on the 292-nm analogue signal (requiring
555 mathematical correction) that could not be compensated by photon counting (available until 2003) and the
556 removal of daylight-induced signal distortions at 313 nm (Trickl et al., 2020a). In principle, this calls for a re-
557 evaluation of the ozone profiles for the wavelength pair 292 nm - 313 nm over the period 2007 to 2011, based on
558 more recent experience in the signal inversion and the performance of the electronic equipment.

559 Vice versa, the lidar measurements helped us to validate the quality of the sonde measurements. Quite good
560 agreement could be achieved by applying an altitude-independent offset correction to the ozone values that
561 strongly varies from sonde to sonde. Most of the ozone differences the two sites are limited to altitudes below 2
562 km. Thus, the differences between Zugspitze and MOHp (at 3 km) reported earlier by Scheel (see Introduction)
563 are not caused by systematic differences in air composition at both sites. As can be seen from the figures
564 presented in this paper the shifted ozone mixing ratios for the sonde and the Zugspitze ozone mostly agrees to
565 within ±3 ppb. Given the frequently substantially higher ozone offsets of the MOHp sondes a recalibration of the
566 archived sonde data based on comparisons with the Zugspitze or UFS in-situ data is advisable despite the

14

567 considerable distance between the sites. Such a recalibration should be avoided in the presence of pronounced

568 ozone structure around the station altitudes which could account for by elevated uncertainties.

569 The comparisons for the three years 2000-2001, 2009 and 2018 reveal just minor performance change of the

570 MOHp sonde over the years, with a variation of the annual average offset by about ±2 ppb. We found a negative

571 average offset of −3.64 ppb ± 3.72 ppb (standard deviation) with respect to the IFU ozone DIAL over all three

572 years. It is reasonable to assume that this offset is applicable to the entire tropospheric time series of the MOHp

573 sondes. This performance is within the uncertainty range of the literature cited in the Introduction.

574 Remaining tasks for the lidar are a substantial reduction of the solar background at 313.2 nm in summer and to

575 enhance the moderate 291.8-nm backscatter signal in the upper troposphere. Further reduction of the residual

576 solar background is difficult since the spectral filtering is already quite narrow. However, replacement of the

577 rather aged (and partly contaminated) primary mirror of the far-field receiver could help by reducing the

578 background radiation reflected into the detection system. As mentioned longer averaging is advisable. By longer

579 averaging, the performance under low-aerosol conditions could almost reach that of in-situ measurements in a

580 major part of the troposphere. Single-photon counting can also be helpful for longer averaging times, as

581 demonstrated for our Raman lidar (Klanner et al., 2021). The noise level for counting is still lower than that of

582 the meanwhile outstanding transient digitizers (Trickl et al., 2020a).

583 **5 Data availability**

584 Lidar data and information on the lidar systems can be obtained on request from the IMK-IFU authors of this

585 paper (thomas@trickl.de, hannes.vogelmann@kit.edu). The 313-nm aerosol backscatter coefficients are archived

586 in the EARLINET data base, accessible through the ACTRIS data portal http://actris.nilu.no/. The

587 Hohenpeißenberg ozone and humidity data are stored in the NDACC data archive (https://www-

588 air.larc.nasa.gov/missions/ndacc/data.html#). The data of the FIRMOS campaign is available via the ESA

589 campaign dataset website https://earth.esa.int/eogateway/campaigns/firmos. The hourly Zugspitze and UFS

590 ozone data are available at the World Data Center for Reactive Gases (WDCRG: https://ebas.nilu.no/) and the

591 TOAR data base (Schultz et al., 2017).

592 **6 Author statement**

593 TT carried out most lidar measurements after spring 1997, following U. Kempfer and H. Eisele. He led the

594 technical development of two ozone DIAL systems since 1990. HV was involved in the system upgrading since

595 2007 and was responsible for the lidar operation during FIRMOS. DC and CW launched several ECC sondes at

596 IMK-IFU in February 2019. MA and WS carried out the MOHp ozone sonde measurements. LR performed

597 ozone in-situ measurements at UFS. MS provided LAGRANTO backward trajectories.

598 **7 Competing interests**

599 The authors declare that they have no conflict of interest.

References

ATMOFAST: Atmosphärischer Ferntransport und seine Auswirkungen auf die Spurengaskonzentrationen in der freien Troposphäre über Mitteleuropa (Atmospheric Long-range Transport and its Impact on the Trace-gas Composition of the Free Troposphere over Central Europe), Project Final Report, T. Trickl, co-ordinator, M. Kerschgens, A. Stohl, and T. Trickl, subproject co-ordinators, funded by the German Ministry of Education and Research within the programme "Atmosphärenforschung 2000", http://www.trickl.de/ATMOFAST.htm, 130 pp., 2005 (in German), with revised publication list of 2012

Ancellet, G., Pelon, J., Beekmann, M., Papayannis, A., and Mégie, G.: Ground-Based Lidar Studies of Ozone Exchanges Between the Stratosphere and the Troposphere, J. Geophys. Res., 96, 22401-22421, 1991.

Ancellet, G., Godin-Beekmann, S., Smit, H. G. J., Stauffer, R. M., Van Malderen, R., Bodichon, R., and Pazmiño, A.: Homogenization of the Observatoire de Haute Provence electrochemical concentration cell (ECC) ozonesonde data record: comparison with lidar and satellite observations, Atmos. Meas. Tech., 15, 3105–3120, 2022.

Attmannspacher, W., and Dütsch, H.: 2nd International Ozone Sonde Intercomparison at the Observatory of Hohenpeissenberg, Berichte des Deutschen Wetterdienstes 157, 1981.

Beekmann, M., Ancellet, G., Mégie, G., Snit, H. G. J., and Kley, D.: Intercomparison Campaign of Vertical Ozone Profiles Including Electrochemical Sondes of ECC and Brewer-Mast Type and a Ground Based UV-Differential Absorption Lidar, J. Atmos. Chem., 19, 259-288, 1994.

Belotti, C., Barbara, F., Barucci, M., Bianchini, G., D'Amato, F., Del Bianco, S., Di Natale, G., Gai, M., Montori, A.,, Pratesi., F., Rolf, C., Sussmann, R., Trickl, T., Viciani, S., Vogelmann, H., Palchetti, L.: The Far-Infrared Radiation Mobile Observation System for spectral characterisation of the atmospheric emission, Atmos. Meas. Tech., 16, 2511–2529, https://doi.org/10.5194/amt-16-2511-2023, 2023.

Brabec, M.: Backscatter and Humidity Measurements in Cirrus and Dust Clouds using Balloon Sondes, Ph.D. thesis, Eidgenössische Technische Hochschule, Zürich (Switzerland), 96 pp., 2011.

Brewer, A. W., and Milford, J. R.: The Oxford-Kew ozone sonde, Proc. R. Soc. Lond. A, 256, 470–495 [available at http://doi.org/10.1098/rspa.1960.0120], 1960.

644 Browell, E. V., Danielsen, E. F., Ismail, S., Gregory, G. L., and Beck, S. M.: Tropopause Fold Structure
645 Determined From Airborne Lidar and in Situ Measurements, J. Geophys. Res., 92, 2112-2120, 1987.

646 Carnuth, W., and Trickl, T.: Transport studies with the IFU three-wavelength aerosol lidar during the VOTALP
647 Mesolcina experiment, Atmos. Environ., 34, 1425-1434, 2000.

648 Carnuth, W., Kempfer, U., and Trickl, T.: Highlights of the tropospheric lidar studies at IFU within the TOR
649 project, Tellus B, 54, 163-185, 2002.

650 Claude, H., Hartmannsgruber, R., and Köhler, U.: Measurement of atmospheric profiles using the Brewer-Mast
651 sonde, World Meteorological Organization, Global Ozone Res. and Monit. Proj. Report No. 17, WMO/TD No.
652 179, Geneva (Switzerland), [see also https://library.wmo.int/index.php?lvl=notice_display&id=11215], 51 pp.,
653 1987.

654 Deshler., T., Stübi, R., Schmidlin, F. J., Mercer, J. L., Smit, H. G. J., Johnson, B. J., Kivi, K., and Nardi, B.:
655 Methods to homogenize electrochemical concentration cell (ECC) ozonesonde measurements across changes in
656 sensing solution concentration or ozonesonde manufacturer, Atmos. Meas. Tech., 10, 2021–2043, 2017.

657 Daumont, D., Brion, J., Charbonnier, J., and Malicet, J.: Ozone UV Spectroscopy I: Absorption Cross-Sections
658 at Room Temperature, J. Atmos. Chem., 15, 145-155, 1992.

659 Davies, W. E., Vaughan, G., and O´Connor, F. M.: Observation of near-zero ozone concentrations in the upper
660 troposphere at mid-latitudes, Geophys. Res. Lett., 25, 1173-1176, 1998.

661 De Backer, H., De Muer, D., and De Sadelaer G.: Comparison of ozone profiles obtained with Brewer-Mast and
662 Z-ECC sensors during simultaneous ascents, J. Geophys. Res., 103, 19,641–19,648,
663 https://doi.org/10.1029/98JD01711, 1998.

664 De Muer, D., and Malcorps, H.: The frequency response of an electrochemical ozone sonde and its application to
665 the deconvolution of ozone profiles, J. Geophys. Res., 89, 1361–1372, 1984.

666 Di Natale, G., Barucci, M., Belotti, C., Bianchini, G., D'Amato, F., Del Bianco, S. Gai, M., Montori, A.,
667 Sussmann, R., Viciani, S., Vogelmann, H., and Palchetti, L.: Comparison of mid-latitude single- and mixed-
668 phase cloud optical depth from co-located infrared spectrometer and backscatter lidar measurements, Atmos.
669 Meas. Tech., 14, 6749–6758, 2021.

670 Dirksen, R. J., Sommer, M., Immler, F. J., Hurst, D. F., Kivi, R., and Vömel, H.: Reference quality upper-air
671 measurements: GRUAN data processing for the Vaisala RS92 radiosonde, Atmos. Meas. Tech., 7, 4463-4490,
672 doi.org/10.5194/amt-7-4463-2014, 2014.

673 Draxler, R., and Hess, G.: An overview of the HYSPLIT_4 modelling system for trajectories, dispersion, and
674 deposition, Aust. Meteorol. Mag., 47, pp. 295-308, 1998.

675 Eisele, H., Trickl, T., and Claude, H.: Lidar als wichtige Ergänzung zur Messung troposphärischen Ozons,
676 Ozonbulletin des Deutsches Wetterdiensts, 44, 2 pp., 1997 (in German).

677 Eisele, H., Scheel, H. E., Sladkovic, R., and Trickl, T.: High-Resolution Lidar Measurements of Stratosphere-
678 Troposphere Exchange, J. Atmos. Sci., 56, 319-330, 1999.

679 Eisele, H., and Trickl, T.: Improvements of the aerosol algorithm in ozone-lidar data processing by use of
680 evolutionary strategies, Appl. Opt., 44, 2638-2651, 2005.

17

681   EUROTRAC: Transport and Chemical Transformation of Pollutants in the Troposphere, Vol. 1, An Overview of
682   the Work of EUROTRAC, P. Borrell and P. M. Borrell, Eds., Springer (Berlin, Heidelberg, New York), ISBN 3-
683   540-66775-X, 474 pp., 1997.

684   Gaudel, A., Ancellet G., and Godin-Beekmann S.: Analysis of 20 years of tropospheric ozone vertical profiles by
685   lidar and ECC at Observatoire de Haute Provence (OHP) at 44° N, 6.7° E, Atmos. Environ., 113, 78-89, 2015.

686   Gaudel, A., Cooper, O. R., Ancellet, G., Barret, B., Boynard, A., Burrows, J. P., Clerbaux, J. P., Coheur, P.-F.,
687   Cuesta, J., Cuevas, E., Doniki, S., Dufour, G., Ebojie, F., Foret, G., Garcia, O., Granados-Muñoz, M. J.,
688   Hannigan, J., Hase, F., Hassler, B., Huang, G., Hurtmans, D., Jaffe, D., Jones, N., Kalabokas, P., Kerridge, B.,
689   Kulawik, S., Latter, B., Leblanc, T., Le Flochmoën, E., Lin, W., Liu, J., Liu, X., Mahieu, E., McClure-Begley,
690   A., Neu, J., Osman, M., Palm, M., Petetin, H., Petropavlovskikh, I., Querel, R., Rahpoe, N., Rozanov, A.,
691   Schultz, M. G., Schwab, J., Siddans, R., Smale, D., Steinbacher, M., Tanimoto, H., Tarasick, D., Thouret, V.,
692   Thompson, A., M., Trickl, T., Weatherhead, E., Wespes, C., Worden, H., Vigouroux, C., Xu, X., Zeng, G.,
693   Ziemke, J.: Tropospheric Ozone Assessment Report: Present-day distribution and trends of tropospheric ozone
694   relevant to climate and global atmospheric chemistry model evaluation, Elem. Sci. Anth., 6, 39, DOI:
695   https://doi.org/ 10.1525/elementa.291, 58 pp., 2018.

696   Grant, W. B., Browell, E. V., Butler, C. F., Fenn, M. A., Clayton, M. B., Hannan, J. R., Fuelberg, H. E., Blake,
697   D. R., Blake, N. J., Gregory, G. L., Heikes, B. G., Sachse, G. W., Singh, H. B., Snow, J., and Talbot, R. W.: A
698   case study of transport of tropical marine boundary layer and lower tropospheric air masses to the northern
699   midlatitude upper troposphere, J. Geophys. Res., 105, 3757-3769, 2000.

700   Hearn, A. G.: The Absorption of Ozone in the Ultra-violet and Visible Regions of the Spectrum, Proc. Phys.
701   Soc., 78, 932-940, 1961.

702   Hersbach, H, Bell, B, Berrisford, P, Simmons, A., Berrisford, P., Dahlgren, P., Horanyi, A., Munoz-Sabater, J.,
703   Nicolas, J., Radu, R., Schepers, D., Soci, C., Villaume, S., Bidlot, J. R., Haimberger, L.; Woollen, J.,
704   Buontempo, C., and Thepaut, J. N.: The ERA5 global reanalysis. Q. J. R. Meteorol Soc., 146, 1999– 2049,
705   https://doi.org/10.1002/qj.3803, 2020.

706   Johnson, B. J., Oltmans, S. J., Vömel, H., Smit, H. G. J., Deshler, T., and Kröger, C.: Electrochemical
707   concentration cell (ECC) ozonesonde pump efficiency measurements and tests on the sensitivity to ozone of
708   buffered and unbuffered ECC sensor cathode solutions, J. Geophys. Res.-Atmos., 107, ACH 8-1–ACH 8-18,
709   https://doi.org/10.1029/2001JD000557, 2002.

710   Jeannet, P., Stübi, R., Levrat, G., Viatte, P., and J. Staehelin, J.: Ozone balloon soundings at Payerne
711   (Switzerland): Reevaluation of the time series 1967–2002 and trend analysis, J. Geophys. Res., 112, D11302,
712   doi:10.1029/2005JD006862, 15 pp., 2007.

713   Kempfer, U., Carnuth, W., Lotz, R., and Trickl, T.: A wide range ultraviolet lidar system for tropospheric ozone
714   measurements: development and application, Rev. Sci. Instrum., 65, 3145-3164, 1994.

715   Kerr, J. B., Fast, H., McElroy, C.T., Oltmans, S.J., Lathrop, J.A., Kyro, E., Paukkunen, A., Claude, H., Köhler,
716   U., Sreedharan, C.R., akao T., and Tsukagoshi, Y.: The 1991 WMO International Ozonesonde Intercomparison
717   at Vanskoy, Canada. Atmos.–Ocean, 32, 685–716, https://doi.org/10.1080/07055900.1994.9649518, 1994.

Klanner, L., Höveler, K., Khordakova, D., Perfahl, M., Rolf, C., Trickl, T., and Vogelmann, H.: A powerful lidar system capable of 1 h measurements of water vapour in the troposphere and the lower stratosphere as well as the temperature in the upper stratosphere and mesosphere, Atmos. Meas. Tech., 14, 531-555, 2021.

Klausen, J., Zellweger, C., Buchmann, B., and Hofer, P.: Uncertainty and bias of surface ozone measurements at selected Global Atmospheric Watch sites, J. Geophys. Res., 108, 4622, doi: 10.1029/2003JD003710, 17 pp., 2003.

Kley, D., Beck, J., Grennfelt, P. I., Hov, O., and Penkett, S. A.: Tropospheric Ozone Research (TOR) A Sub-Project of EUROTRAC, J. Atmos. Chem., 28, 1–9, 1997.

Kley, D., Crutzen, P. J., Smit, H. G. J., Vömel, H., Oltmans, S., Grassl, H., and Ramanathan, V.: Observations of Near-Zero Ozone Concentrations Over the Convective Pacific: Effects on Air Chemistry, Science, 274, 230-233, 1996.

Komhyr, W.D.: Electrochemical concentration cells for gas analysis, Ann. Geoph., 25, 203–210, 1969.

Komhyr, W. D., Barnes, R. A., Brothers, G. B., Lathrop, J. A., and Opperman, D. P.: Electrochemical concentration cell ozonesonde performance evaluation during STOIC 1989, J. Geophys. Res., 100, 9231–9244, https://doi.org/10.1029/94JD02175, 1995.

Langford, A. O., Masters, C. D., Proffitt, M. H., Hsie, E.-Y., and Tuck, A. F.: Ozone measurements in a tropopause fold associated with a cut-off low system, Geophys. Res. Lett., 23, 2501–2504, 1996.

Logan, J.A., Staehelin, J., Megretskaia, I.A., Cammas, J.-P., Thouret, V., Claude, H., De Backer, H., Steinbacher, M., Scheel, H.-E., Stübi, R., Fröhlich, M., and Derwent, R. (2012), Changes in ozone over Europe: Analysis of ozone measurements from sondes, regular aircraft (MOZAIC) and alpine surface sites, J. Geophys. Res., 117, D09301, doi:10.1029/2011JD016952.

Malicet, J., Daumont, D., Charbonnier, J., Parisse, C., Chakir, A., and Brion, J.: Ozone UV Spectroscopy I: Absorption Cross-Sections and Temperature Dependence, J. Atmos. Chem., 21, 263-273, 1995.

Palchetti, L., Barucci, M., Belotti, C., Bianchini, G., Cluzet, B., D'Amato, F., Del Bianco, S., Di Natale, G., Gai, M., Khordakova, D., Montori, A., Oetjen, H., Rettinger, M., Rolf, C., Schuettemeyer, D., Sussmann, R., Viciani, S., Vogelmann, H., and Wienhold, F. G.: Observations of the downwelling far-infrared atmospheric emission at the Zugspitze observatory, Earth Syst. Sci. Data, 13, 4303–4312, https://doi.org/10.5194/essd-13-4303-2021, 2021.

Parrish, D. D., Derwent, R. G., Steinbrecht, W., Stübi, R., Van Malderen, R., Steinbacher, M., Trickl, T., Ries, L., and Xu, X.: Zonal Similarity of Long-term Changes and Seasonal Cycles of Baseline Ozone at Northern Mid-latitudes, J. Geophys. Res., 125, e2019JD031908, https://doi.org/10.1029/2019JD031908, 19 pp., 2020.

Schultz, M. G., Schröder, S., Lyapina, O., Cooper, O., Galbally, I., Petropavlovskikh, I., von Schneidemesser, E., Tanimoto, H., Elshorbany, Y., Naja, M., Seguel, R. J., Dauert, U., Eckhardt, P., Feigenspan, S., Fiebig, M., Hjellbrekke, A.-G., Hong, Y.-D., Kjeld, P. C., Koide, H., Lear, G., Tarasick, D., Ueno, M., Wallasch, M., Baumgardner, D., Chuang, M.-T., Gillett, R., Lee, M., Molloy, S., Moolla, R., Wang, T., Sharps, K., Adame, J. A., Ancellet, G., Apadula, F., Artaxo, P., Barlasina, M. E., Bogucka, M., Bonasoni, P., Chang, L., Colomb, A., Cuevas-Agulló, E., Cupeiro, M., Degorska, A., Ding, A., Fröhlich, M., Frolova, M., Gadhavi, H., Gheusi, F., Gilge, S., Gonzalez, M. Y., Gros, V., Hamad, S. H., Helmig, D., Henriques, D., Hermansen, O., Holla, R., Hueber, J., Im, U., Jaffe, D. A., Komala, N., Kubistin, D., Lam, K.-S., Laurila, T., Lee, H., Levy, I., Mazzoleni,

C., Mazzoleni, L. R., McClure-Begley, A., Mohamad, M., Murovec, M., Navarro-Comas, M., Nicodim, F., Parrish, D., Read, K. A., Reid, N., Ries, L., Saxena, P., Schwab, J. J., Scorgie, Y., Senik, I., Simmonds, P., Sinha, V., Skorokhod, A. I., Spain, G., Spangl, W., Spoor, R., Springston, S. R., Steer, K., Steinbacher, M., Suharguniyawan, E., Torre, P., Trickl, T., Weili, L., Weller, R., Xiaobin, X., Xue, L., and Zhiqiang, M.: Tropospheric Ozone Assessment Report: Database and Metrics Data of Global Surface Ozone Observations, Elem. Sci. Anth., 5, 58, DOI: https://doi.org/ 10.1525/elementa.244, 25 pp., 2017.

Reichardt, J., Ansmann, A., Serwazi, M., Weitkamp, C., and Michaelis, W.: Unexpectedly low ozone concentration in midlatitude tropospheric ice clouds: A case study, Geophys. Res.Lett., 23, 1929-1932, 1996.

Smit, H. G. J, Straeter, W., Johnson, B. J., Oltmans, S. J., Davies, J., Tarasick, D. W., Hoegger, B., Stubi, R., Schmidlin, F. J., Northam, T., Thompson, A. M., Witte, J. C., Boyd, I., and Posny, F.: Assessment of the Performance of ECC-ozonesondes under Quasi-flight Conditions in the Environmental Simulation Chamber: Insights from the Jülich Ozone Sonde Intercomparison Experiment (JOSIE), J. Geophys. Res., 112, D19306, doi:10.1029/2006JD007308, 18 pp., 2007.

Smit, H.G.J., and ASOPOS panel: Quality assurance and quality control for ozonesonde measurements in GAW, World Meteorological Organization, GAW Report No. 201, Geneva (Switzerland). [Available online at https://library.wmo.int/doc_num.php?explnum_id=7167], 100 pp., 2014.

Smit, H.G.J., and Thompson, A.M.: Ozonesonde Measurement Principles and Best Operational Practices: ASOPOS 2.0 (Assessment of Standard Operating Procedures for Ozonesondes), World Meteorological Organization, GAW Report No. 268, Geneva (Switzerland). [Available online at https://library.wmo.int/doc_num.php?explnum_id=10884], 172 pp., 2021.

Stauffer, R.M., Thompson, A.M., Kollonige, D.E., Tarasick, D.W., Van Malderen, R., Smit, H.G.J., Vömel, H., Morris, G.A., Johnson, B.J., Cullis, P.D., Stübi, R., Davies, J., and Yan.: An Examination of the Recent Stability of Ozonesonde Global Network Data, Earth and Space Science, 9 (10), e2022EA002459, [available online at https://doi.org/10.1029/2022EA002459], 2022.

Stein, A. F., Draxler, R. R, Rolph, G. D., Stunder, B. J. B., Cohen, M. D., and Ngan, F.: NOAA's HYSPLIT atmospheric transport and dispersion modeling system, Bull. Amer. Meteor. Soc., 96, 2059-2077, 2015.

Steinbrecht, W., Schwarz, R., and Claude, H.: New pump correction for the Brewer-Mast ozone sonde: determination from experiment and instrument intercomparisons, J. Atmos. Ocean. Tech., 15, 144–156, 1998.

Stohl, A., and Trickl, T.: A textbook example of long-range transport: Simultaneous observation of ozone maxima of stratospheric and North American origin in the free troposphere over Europe, J. Geophys. Res., 104, 30445-30462, 1999.

Stohl, A., Bonasoni, P., Cristofanelli, P., Collins, W., Feichter, J., Frank, A., Forster, C., Gerasopoulos, E., Gäggeler, H., James, P., Kentarchos, T., Kromp-Kolb, H., Krüger, B., Land, C., Meloen, J., Papayannis, A., Priller, A., Seibert, P., Sprenger, M., Roelofs, G. J., Scheel, H. E., Schnabel, C., Siegmund, P., Tobler, L., Trickl, T., Wernli, H., Wirth, V., Zanis, P., and Zerefos, C.: Stratosphere-troposphere exchange - a review, and what we have learned from STACCATO, J. Geophys. Res., 108, 8516, doi:10.1029/2002JD002490, STA 1, 15 pp., 2003.

Stübi, R., Levrat, G., Hoegger, B., Pierre Viatte, P., Staehelin, J., Schmidlin, F.J.: In-flight comparison of Brewer-Mast and electrochemical concentration cell ozonesondes, J. Geophys. Res., 113, D13302, https://doi.org/10.1029/2007JD009091, 2008.

Tarasick, D. W., Davies, J., Anlauf, K., Watt, M., Steinbrecht, W., Claude H.-J.: Laboratory investigations of the response of Brewer-Mast ozonesondes to tropospheric ozone, J. Geophys. Res., 107, ACH 14-1 – 14-10, https://doi.org/10.1029/2001JD001167, 2002.

Tarasick, D. W., Davies, J., Smit, H. G. J., and Oltmans, S. J.: A re-evaluated Canadian ozonesonde record: measurements of the vertical distribution of ozone over Canada from 1966 to 2013, Atmos. Meas. Tech., 9, 195–214, https://doi.org/10.5194/amt-9-195-2016, 2016.

Tarasick, D., Galbally, I. E., Cooper, O. R., Schultz, G M., Ancellet, G., Leblanc, T., Wallington, T. J., Ziemke, J., Liu, X., Steinbacher, M., Staehelin, J., Vigouroux, C., Hannigan, J., García, O., Foret, G., Zanis, P., Weatherhead, E., Petropavlovskikh, I., Worden, H., Osman, M., Liu, J., Chang, K.-L., Gaudel, A., Lin, M., Granados-Muñoz, M., Thompson, A. M., Oltmans, S. J., Cuesta, J., Dufour, G., Thouret, V., Hassler, B., Trickl, T., and Neu, J. L.: Tropospheric Ozone Assessment Report: Tropospheric ozone from 1877 to 2016, observed levels, trends and uncertainties, Elem. Sci. Anth., **7**, Article 39, DOI: https://doi.org/10.1525/elementa.376, 72 pp. (plus 56 pp. of supplemental material), 2019.

Tarasick, D. W., Smit, H. G. J., Thompson, A. M., Morris, G. A., Witte, J. C., Davies, J., Davies, J., Nakano, T., Van Malderen, R., Stauffer, R. M., Johnson, B. J., Stubi1, R., Oltmans, S. J., and Vömel, H.: Improving ECC ozonesonde data quality: Assessment of current methods and outstanding issues, Earth and Space Science, 8, e2019EA000914. https://doi.org/10.1029/2019EA000914, 27 pp., 2021.

TESLAS: Tropospheric Environmental Studies by Laser Sounding (TESLAS), in: Transport and Chemical Transformation of Pollutants in the Troposphere, Vol. 8, Instrument Development for Atmospheric Research and Monitoring, J. Bösenberg, D. Brassington, and P. C. Simon, Eds., Springer (Berlin, Heidelberg, New York), ISBN 3-540-62516-X, 1-203, 1997.

Thompson, A. M., Smit, H. G. J., Witte, J. C., Stauffer, R. M., Johnson, B. J., Morris, G., von der Gathen, P., Van Malderen, R., Davies, J., Piters, A., Allaart, M., Posny, F., Kivi, R., Cullis, P., Hoang Anh, N. T., Corrales, E., Machinini, T., da Silva, F. R., Paiman, G., Thiong'o, K., Zainal, Z., Brothers, G. B., Wolff, K. R., Nakano, T., Stübi, R., Romanens, G., Coetzee, G. J. R., Diaz, J. A., Mitro, S., Mohamad, M., and Ogino, S.: Ozonesonde Quality Assurance: The JOSIE–SHADOZ (2017) Experience, Bulletin of the American Meteorological Society, 100, 155-171, 2019.

Trickl, T., Cooper, O. R., Eisele, H., James, P., Mücke, R., and Stohl, A.: Intercontinental transport and its influence on the ozone concentrations over central Europe: Three case studies, J. Geophys. Res., 108, D12, 8530, 10.1029/2002JD002735, STA 15, 23 pp., 2003.

Trickl, T., Feldmann, H., Kanter, H.-J., Scheel, H. E., Sprenger, M., Stohl, A., and Wernli, H.: Deep stratospheric intrusions over Central Europe: case studies and climatological aspects, Atmos. Chem. Phys., 10, 499-524, 2010.

Trickl, T., Eisele, H., Bärtsch-Ritter, N., Furger, M., Mücke, R., Sprenger, M., and Stohl, A.: High-ozone layers in the middle and upper troposphere above Central Europe: potential import from the stratosphere along the subtropical jet stream, Atmos. Chem. Phys., 11, 9343-9366; 5-p. Supplement, 2011.

Trickl, T., Vogelmann, H., Giehl, H., Scheel, H. E., Sprenger, M., and Stohl, A.: How stratospheric are deep stratospheric intrusions? Atmos. Chem. Phys., 14, 9941-9961, 2014.

834   Trickl, T., Vogelmann, H., Flentje, H., and Ries, L.: Stratospheric ozone in boreal fire plumes – the 2013 smoke
835   season over Central Europe, Atmos. Chem. Phys., 15, 9631-9649, 2015.

836   Trickl, T., Vogelmann, H., Fix, A., Schäfler, A., Wirth, M., Calpini, B., Levrat, G., Romanens, G., Apituley, A.,
837   Wilson, K. M., Begbie, R., Reichardt, J., Vömel, H. and Sprenger, M.: How stratospheric are deep stratospheric
838   intrusions into the troposphere? LUAMI 2008, Atmos. Chem. Phys, 16, 8791-8815, 2016.

839   Trickl, T., Neidl, F., Giehl, H., Perfahl, M., and Vogelmann, H.: Three decades of tropospheric ozone lidar
840   development at Garmisch-Partenkirchen, Atmos. Meas. Tech., 13, 6357-6390, 2020a.

841   Trickl, T., Vogelmann, H., Ries, L., and Sprenger, M.: Very high stratospheric influence observed in the free
842   troposphere over the Northern Alps – just a local phenomenon? Atmos. Chem. Phys., 20, 243-266, 2020b.

843   Trickl, T., Couret, C., Ries, L., and Vogelmann, H.: Zugspitze ozone 1978 – 2020: The role of stratosphere-
844   troposphere transport, Atmos. Chem.Phys., 23, 8403–8427, 2013; Corrigendum: https://doi.org/10.5194/acp-23-
845   8403-2023-corrigendum

846   Vaisala: Vaisala Radiosonde RS41 Measurement Performance, White Paper, Vaisala, Helsinki (Finland),
847   https://www.vaisala.com/sites/default/files/documents/WEA-MET-RS41-Performance-White-paper-
848   B211356EN-B-LOW-v3.pdf, 28 pp. (accessed 7 September 2019), 2017.

849   Van Malderen, R., Allaart, M. A. F., De Backer, H., Smit, H. G. J., and De Muer, D.: On instrumental errors and
850   related correction strategies of ozonesondes: possible effect on calculated ozone trends for the nearby sites Uccle
851   and De Bilt, Atmos. Meas. Tech., 9, 3793–3816, 2016

852   Viallon, J., Lee, S., Moussay, P., Tworek, K., Peterson, M., and Wielgosz, R. I.: Accurate measurements of
853   ozone absorption cross-sections in the Hartley band, Atmos. Meas. Tech., 8, 1245-1257, 2015.

854   Völger, P., Bösenberg, J., and Schult, I.: Scattering Properties of Selected Model Aerosols Calculated at UV-
855   Wavelengths: Implications for DIAL Measurements of Tropospheric Ozone, Beitr. Phys. Atmosph., 69, 177-
856   187, 1996.

857   Vömel, H., David, D. E., and Smith, K.: Accuracy of tropospheric and stratospheric water vapor measurements
858   by the cryogenic frost point hygrometer: Instrumental details and observations, J. Geophys. Res., 112, D08305,
859   doi: 10.1029/2006JD007224, 14 pp., 2007.

860   Vömel, H., Naebert, T., Dirksen, R., and Sommer, M.: An update on the uncertainties of water vapor
861   measurements using Cryogenic Frostpoint Hygrometers, Atmos. Meas. Tech., 9, 3755-3768, 2016.

862   Vömel, H., Smit, H. G. J., Tarasick, D., Johnson, B., Oltmans, S. J., Selkirk, H., Thompson, A. M., Stauffer, R.
863   M., Witte, J. C., Davies, J., van Malderen, R., Morris, G. A., Nakano, T., and Stübi, R.: A new method to correct
864   the electrochemical concentration cell (ECC) ozonesonde time response and its implications for "background
865   current" and pump efficiency, Atmos. Meas. Tech., 13, 5667–5680, 2020.

866   Vogelmann, H. and Trickl, T.: Wide-Range Sounding of Free-Tropospheric Water Vapor with a Differential-
867   Absorption Lidar (DIAL) at a High-Altitude Station, Appl. Opt., 47, 2116-2132, 2008.

868   Vogelmann, H., Sussmann, R., Trickl, T., and Borsdorff, T.: Intercomparison of atmospheric water vapor
869   soundings from the differential absorption lidar (DIAL) and the solar FTIR system on Mt. Zugspitze, Atmos.
870   Meas. Tech., 4, 835-841, 2011.

871 Vogelmann, H., Sussmann, R., Trickl, T., and Reichardt, A.: Spatiotemporal variability of water vapor
872 investigated using lidar and FTIR vertical soundings above the Zugspitze, Atmos. Chem. Phys., 14, 3135-3148,
873 2015.

874 VOTALP II: Vertical Ozone Transport in the Alps II, Final Report for the European Union, Contract Nr.: ENV4
875 CT970413, Reporting Period 1/3/1998-29/2/2000, H. Kromp-Kolb, Co-ordinator, Universität für Bodenkultur
876 Wien (Austria), Institut für Meteorologie und Physik, 96 pp., 2000.

877 Wernli, H., and Davies, H.C.: A Lagrangian-based analysis of extratropical cyclones. I: The method and some
878 applications. Q.J.R. Meteorol. Soc., 123: 467-489, https://doi.org/10.1002/qj.49712353811, 1997.

879 Sprenger, M., and Wernli, H.: The LAGRANTO Lagrangian analysis tool – version 2.0, Geosci. Model Dev., 8,
880 2569–2586, https://doi.org/10.5194/gmd-8-2569-2015, 2015.

881 Wotava, G., and Kromp-Kolb, H.: The research project VOTALP – general objectives and main results, Atmos.
882 Environ., 34, 1319-1322, 2000.

883 Yuan, Y., Ries, L., Petermeier, H., Trickl, T., Leuchner, M., Couret, C., Sohmer, R., Meinhardt, F., and Menzel,
884 A.: On the diurnal, weekly, and seasonal cycles and annual trends in atmospheric CO_2 at Mount Zugspitze,
885 Germany, during 1981–2016, Atmos. Chem. Phys., 19, 999–1012, https://doi.org/10.5194/acp-19-999-2019,
886 2019.

887 Zanis, P., Trickl, T., Stohl, A., Wernli, H., Cooper, O., Zerefos, C., Gaeggeler, H., Priller, A., Schnabel, C.,
888 Scheel, H. E., Kanter, H. J., Tobler, L., Kubik, P. W., Cristofanelli, P., Forster, C., James, P., Gerasopoulos, E.,
889 Delcloo, A., Papayannis, A., and Claude, H.: Forecast, observation and modelling of a deep stratospheric
890 intrusion event over Europe, Atmos. Chem. Phys., 3, 763-777, 2003.

891 Zellweger, C., Buchmann, B., Klausen, J., and Hofer, P.: System and Performance Audit of Surface Ozone,
892 Carbon Monoxide and Methane at the Global GAW Station Zugspitze/Hohenpeißenberg, Platform Zugspitze,
893 Germany, Empa-WCC Report 01/1, submitted to the World Meteorological Organization, 49 pp., February
894 2001.

895 Zellweger, C., Klausen, J., and Buchmann, B.,: System and Performance Audit of Surface Ozone, Carbon
896 Monoxide and Methane at the Global GAW Station Zugspitze/Schneefernerhaus, Germany, Empa-WCC Report
897 06/2, submitted to the World Meteorological Organization, 51 pp., June 2006.

898 Zellweger, C., Steinbacher, M., and Buchmann, B., and Steinbrecher, R.: System and Performance Audit of
899 Surface Ozone, Methane, Carbon Dioxide, Nitrous Oxide and Carbon Monoxide at the Global GAW Station
900 Zugspitze-Schneefernerhaus, Germany, submitted to WMO by WMO World Calibration Centre WCC-Empa
901 Empa Dübendorf, Switzerland, 46. pp., WCC-Empa Report 11/2, June 2011.

902 Zellweger, C., Steinbacher, M., Buchmann, B., and Steinbrecher, R.: System and Performance Audit of Surface
903 Ozone, Methane, Carbon Dioxide, Nitrous Oxide and Carbon Monoxide at the Global GAW Station Zugspitze-
904 Schneefernerhaus, Germany, submitted to WMO by WMO World Calibration Centre WCC-Empa Empa
905 Dübendorf, Switzerland, WCC-Empa Report 20/3, September 2020, GAW report 266, 54. pp., 2021.
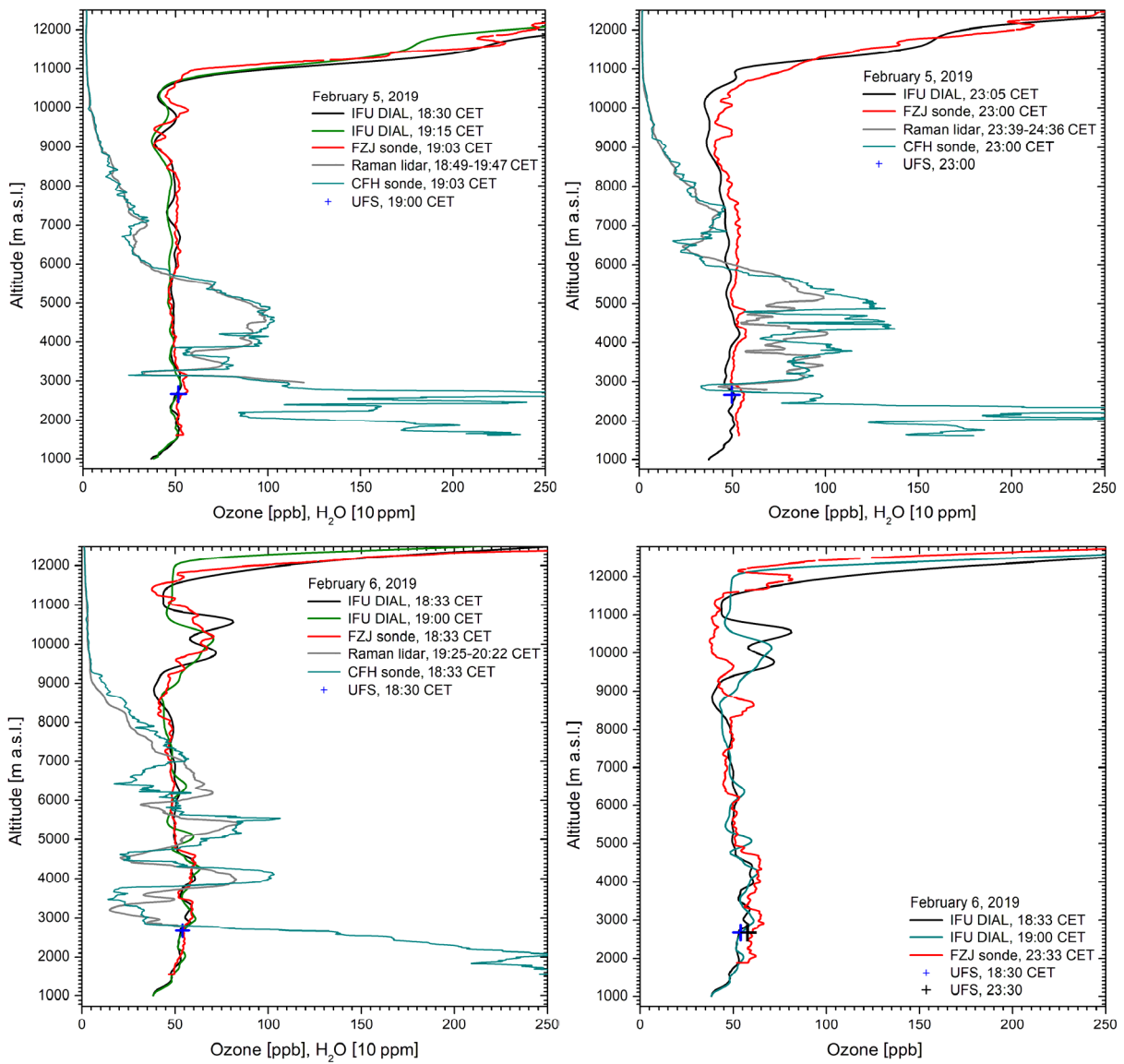
906

907

Figures:
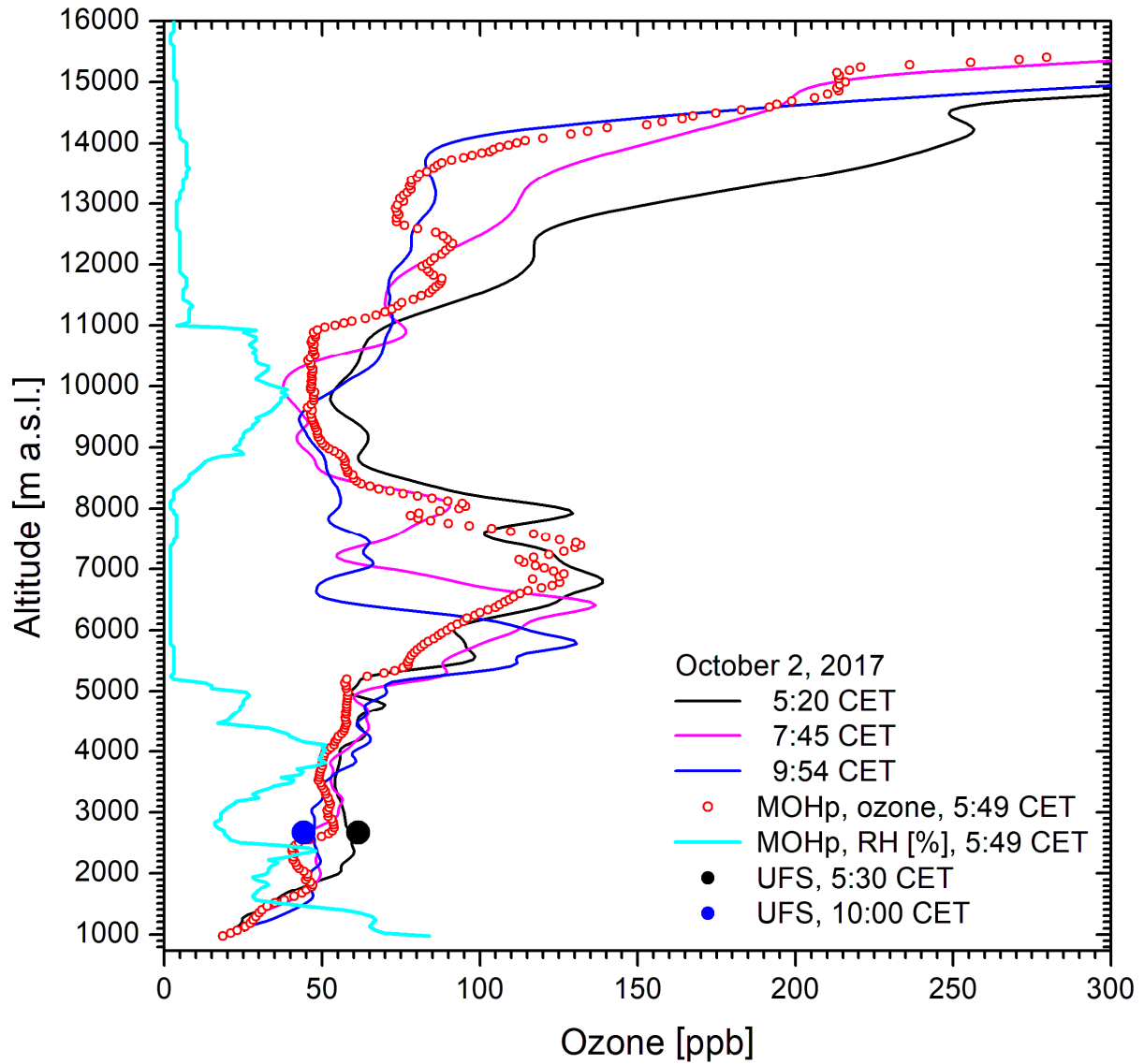
Fig. 1. Ozone measurements at Garmisch-Partenkirchen (IFU, UFS) and Hohenpeißenberg (MOHp) on 2
October 2017; the low relative humidity between 5.2 and 8.3 km (RH = 2 %) verifies the presence of a
stratospheric air intrusion. The time for MOHp is the launch time of the sonde.

Fig. 2. Four ozone measurements on 5 and 6 February 2019 with lidar (IFU), ECC sonde (FZJ) and an in-situ sensor at UFS; for two measurements the FZJ ozone mixing ratios are slightly higher than the lidar results. The fourth FZJ ozone measurement took place much later than the final lidar measurements which resulted in slightly larger differences up to 4.8 km, confirmed by the 23:30-CET measurement at UFS. The lidar results around 10 km on 6 February are uncertain due to a cirrus correction. In order to visualize more details on the complex layering we also show water-vapour mixing ratios for roughly coinciding measurements of the UFS Raman lidar and the FZJ CFH sonde. The tropospheric structures are strongly smoothed for the lidar due to the 1-h data-acquisition time. At 3.3 km 250 ppm corresponds to roughly 5 % RH.
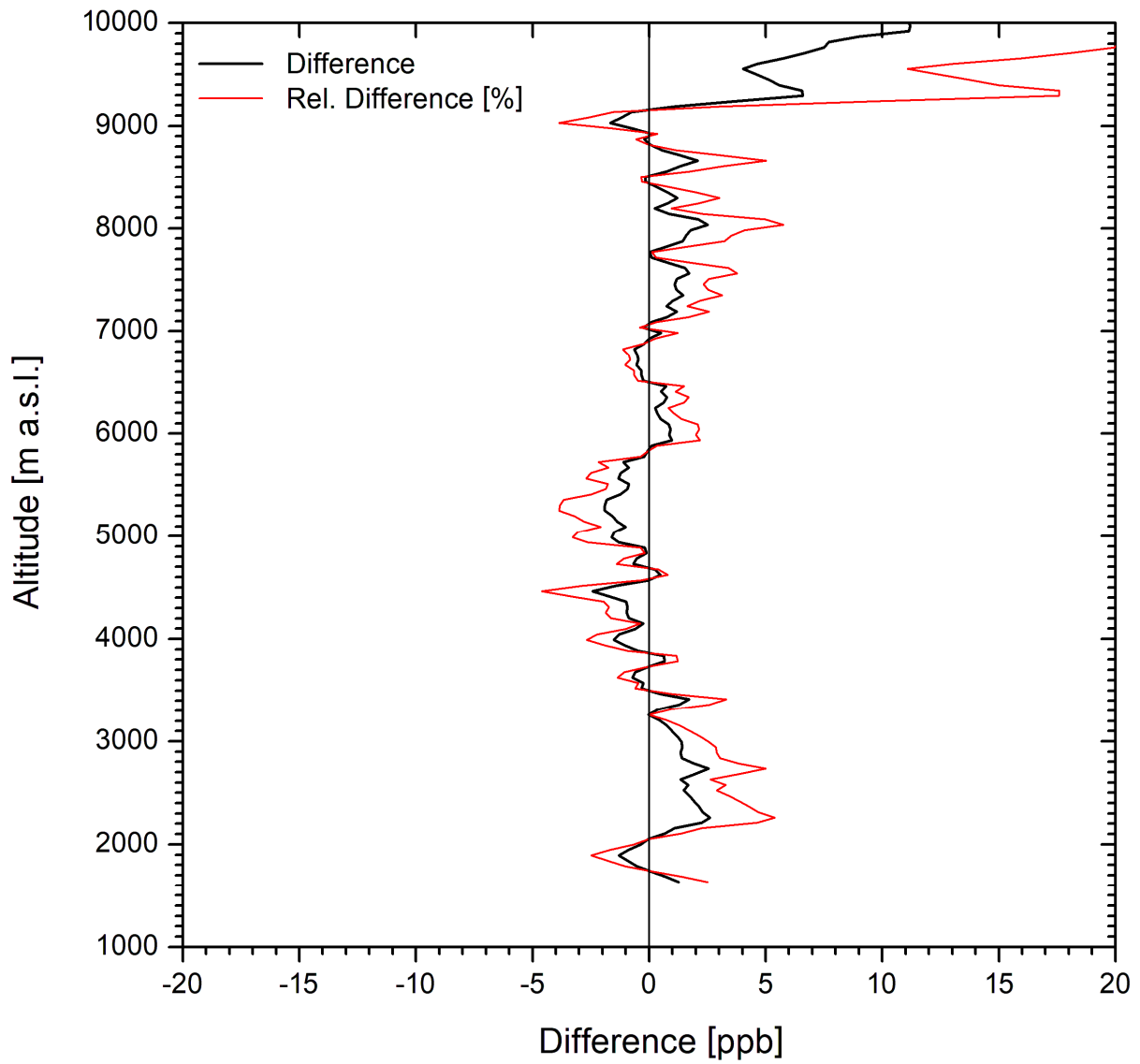
Fig. 3. Averaged differences between FZJ ozone sonde and IMK-IFU lidar for the first three comparisons after a

slight offset correction of the sonde profiles (see text)
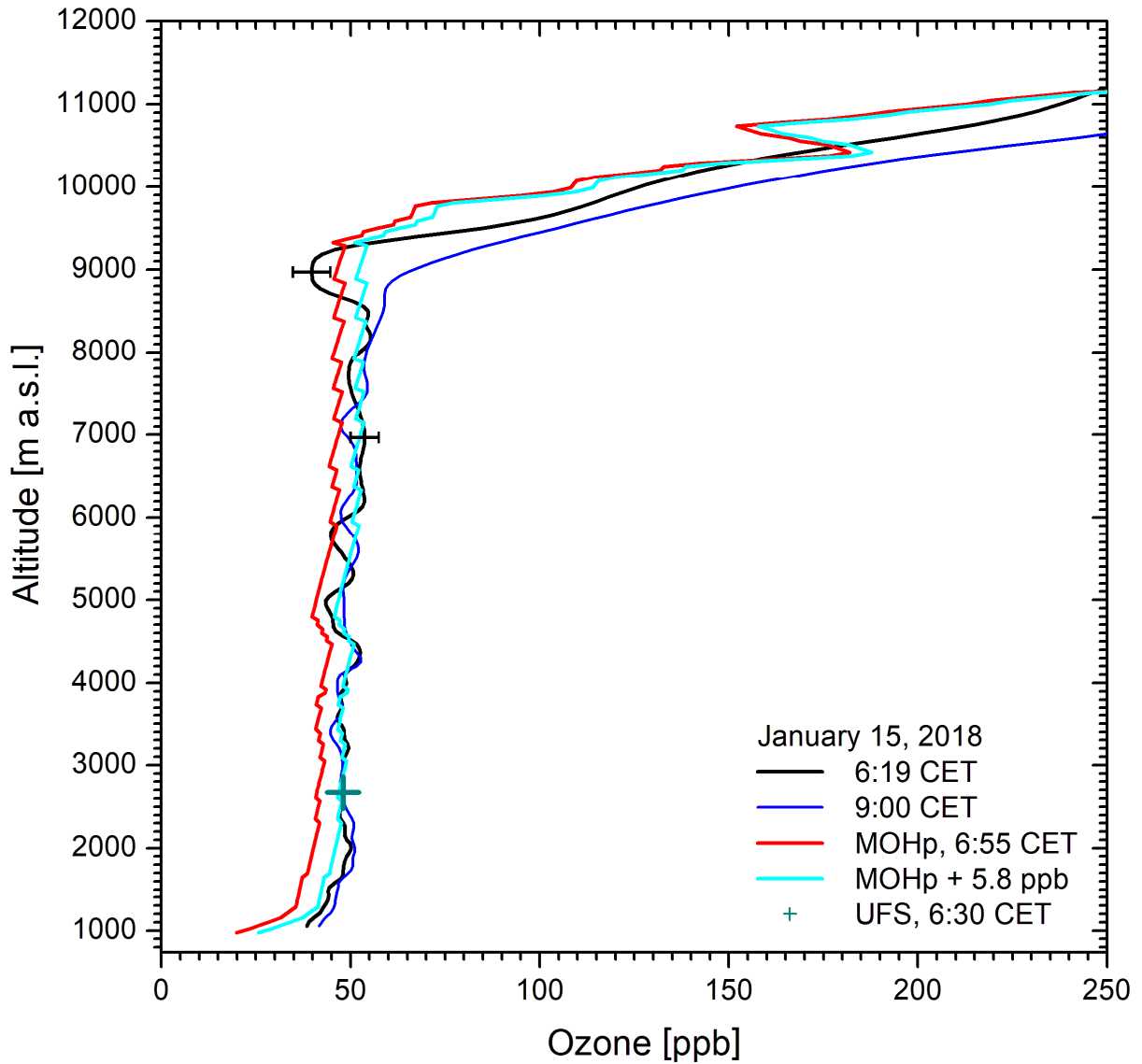
Fig. 4. Ozone measurements on 15 January 2018: The MOHp ozone (red) is also shown shifted by 5.8 ppb to
933   match the lidar ozone and the UFS value (cyan), in part the black, in part the blue curve. Differences exist in the
934   tropopause region, which is frequently the case. The sawtooth structure in the MOHp data is due to insufficient
935   digital resolution in the NDACC data base.
936
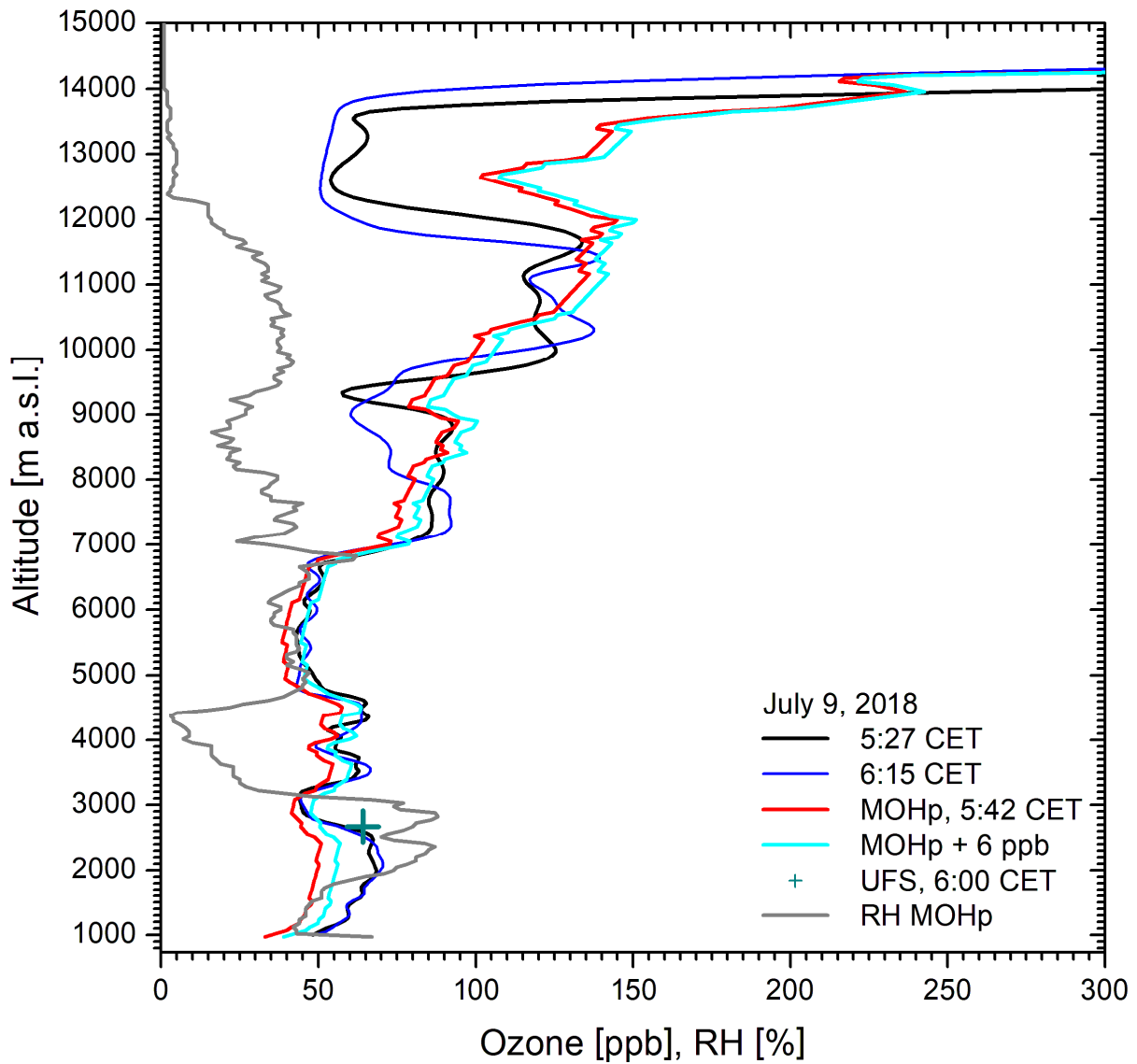
Fig. 5. Summertime ozone measurements (July 9, 2018) with pronounced layering; the sonde ozone (red) is brought to reasonable agreement with the lidar (black curve) above 2.7 km by adding 6 ppb (cyan curve). Above 9 km the air masses are no longer comparable. The particularly strong discrepancy of the UFS in-situ ozone can be explained by orographic lifting of the ozone edge at 2.7 km. The low to moderate RH (grey) in parts of the free troposphere indicates that the elevated ozone values could be due to a stratospheric air component.

944
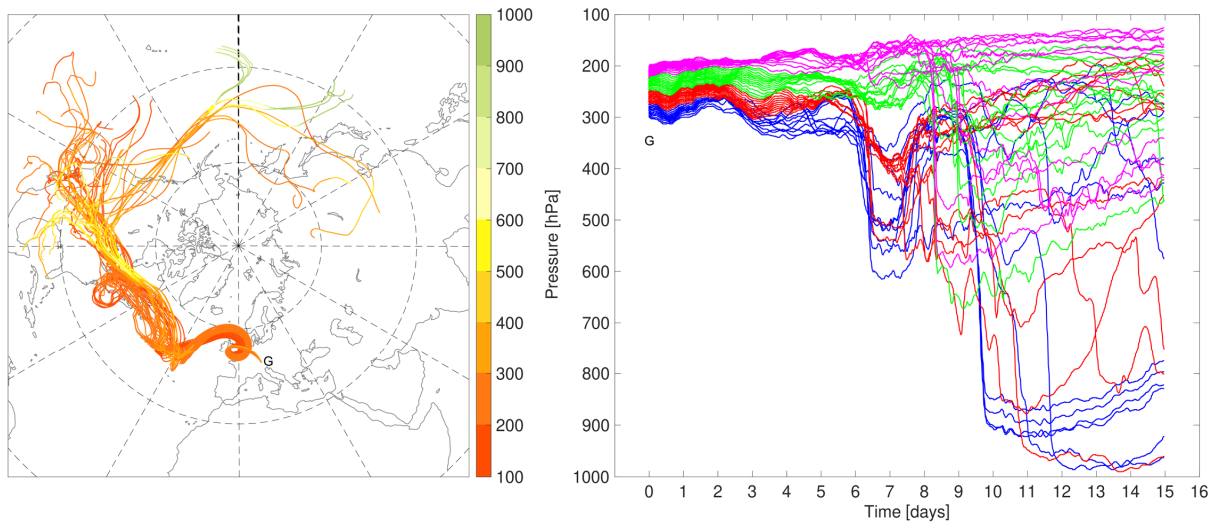
Fig. 6. 350-h LAGRANTO backward trajectories, started above Garmisch-Partenkirchen (G) on 9 July 2018 at 7:00 CET
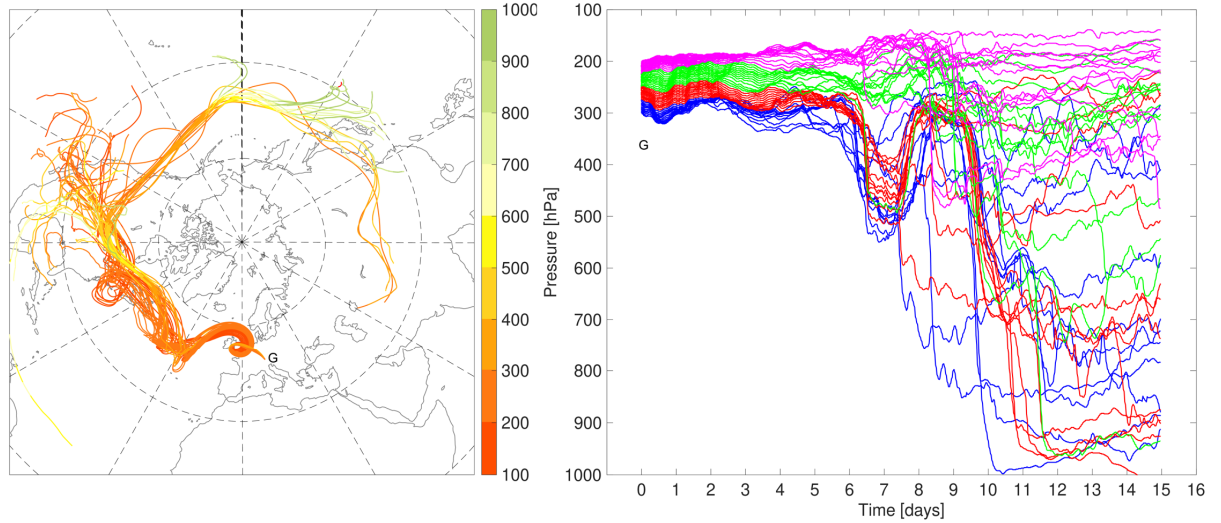
Fig. 7. 350-h LAGRANTO backward trajectories, started above Garmisch-Partenkirchen (G) on 9 July 2018 at 8:00 CET

29
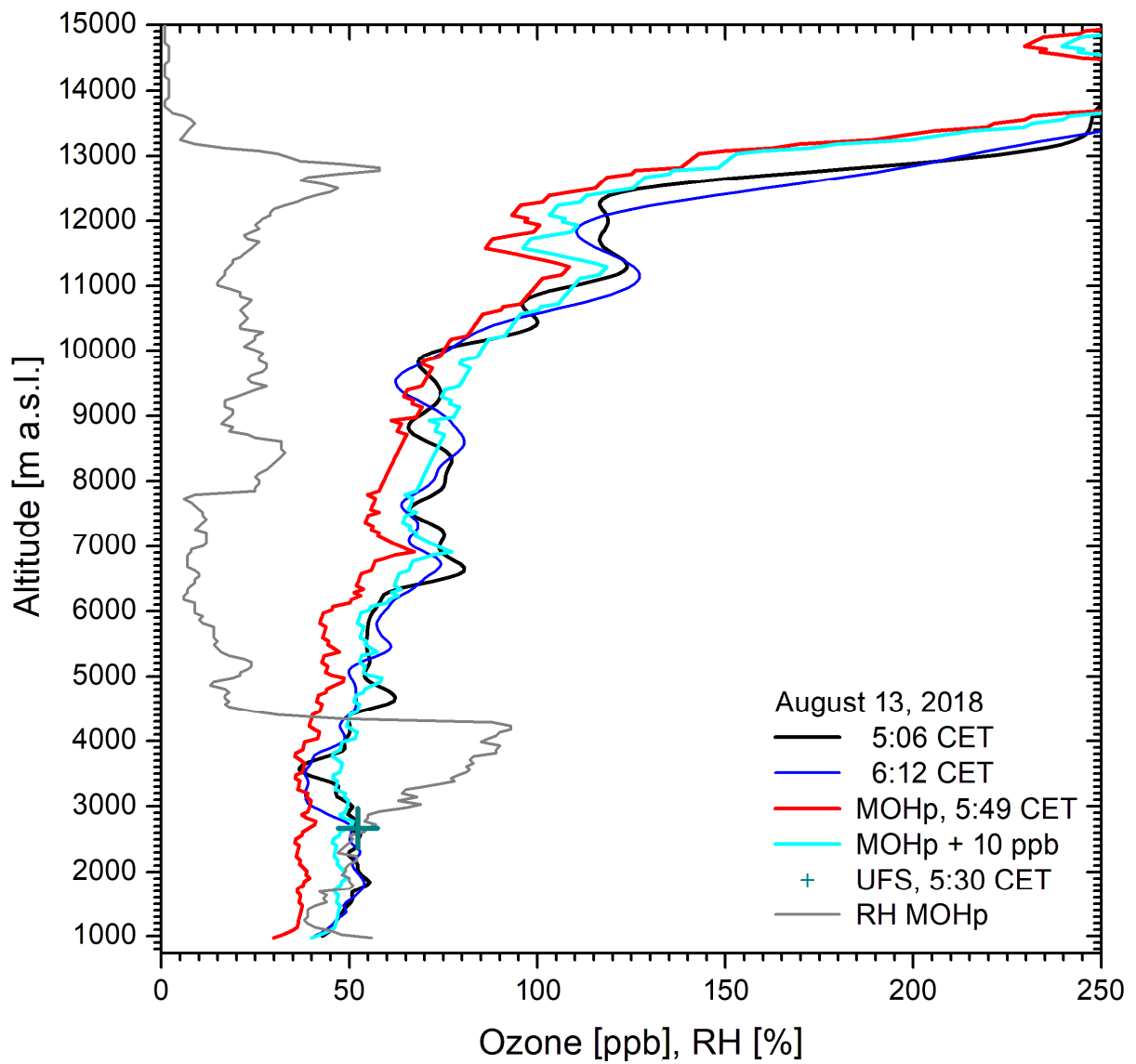
Fig. 8. Ozone measurements on 13 August 2018: The agreement of the shifted MOHp ozone profile (cyan) with the lidar curves is rather good up to 12 km given the high summertime variability. The low to moderate RH above 4.4 km (grey) indicates that the elevated ozone is partially caused by stratospheric air.
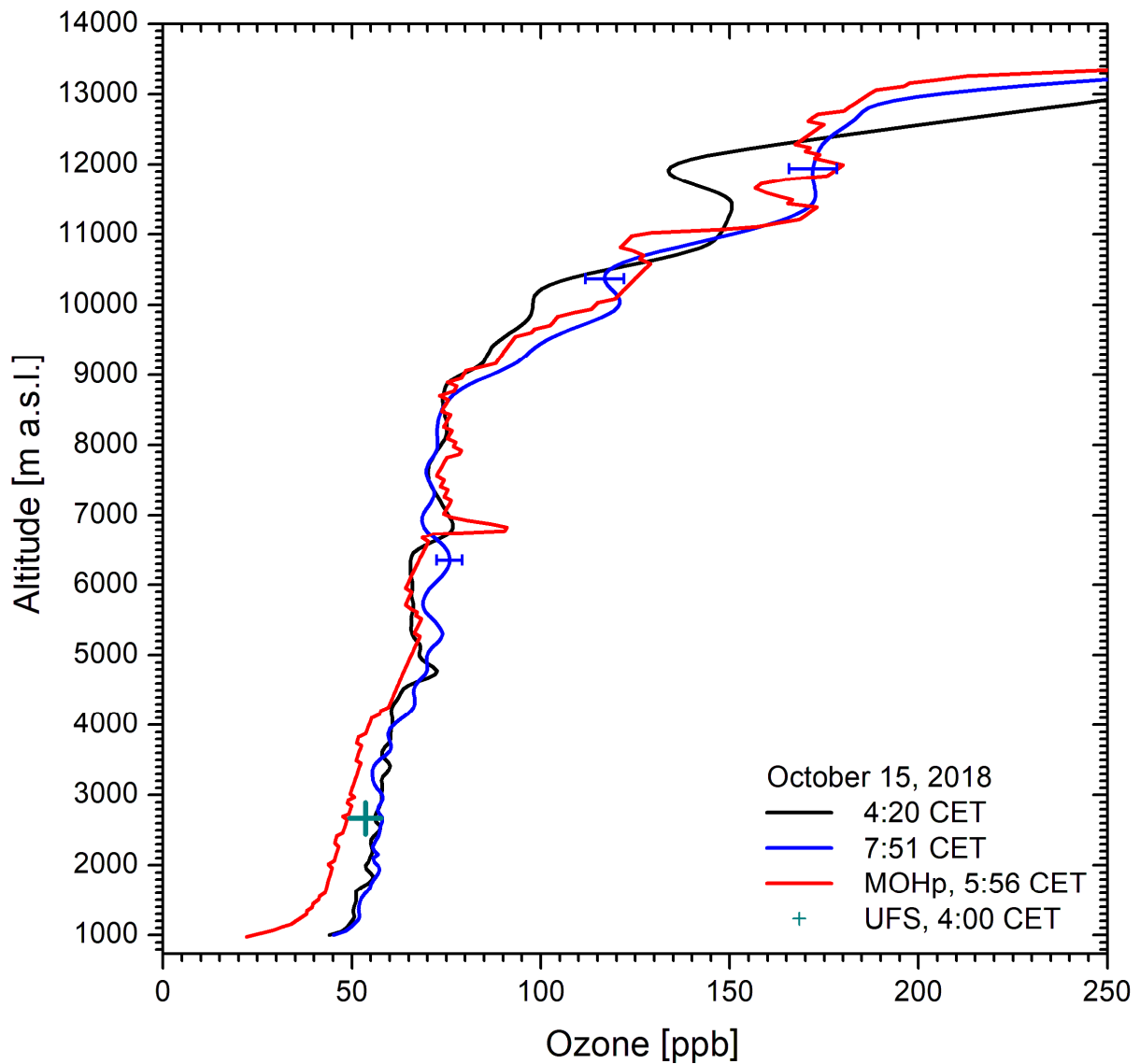
Fig. 9. Ozone measurements on 15 October 2018: The MOHp ozone (red) is not shifted. The agreement above
4.3 km is better with the earlier lidar measurement (black), above 7 km better with the blue curve. The lidar data
are strongly smoothed in the stratosphere, as can be seen from the more detailed ozone structure in the sonde
data. This example is one of the two examples with a pronounced low-altitude discrepancy between lidar and
sonde extending to more the 3 km.
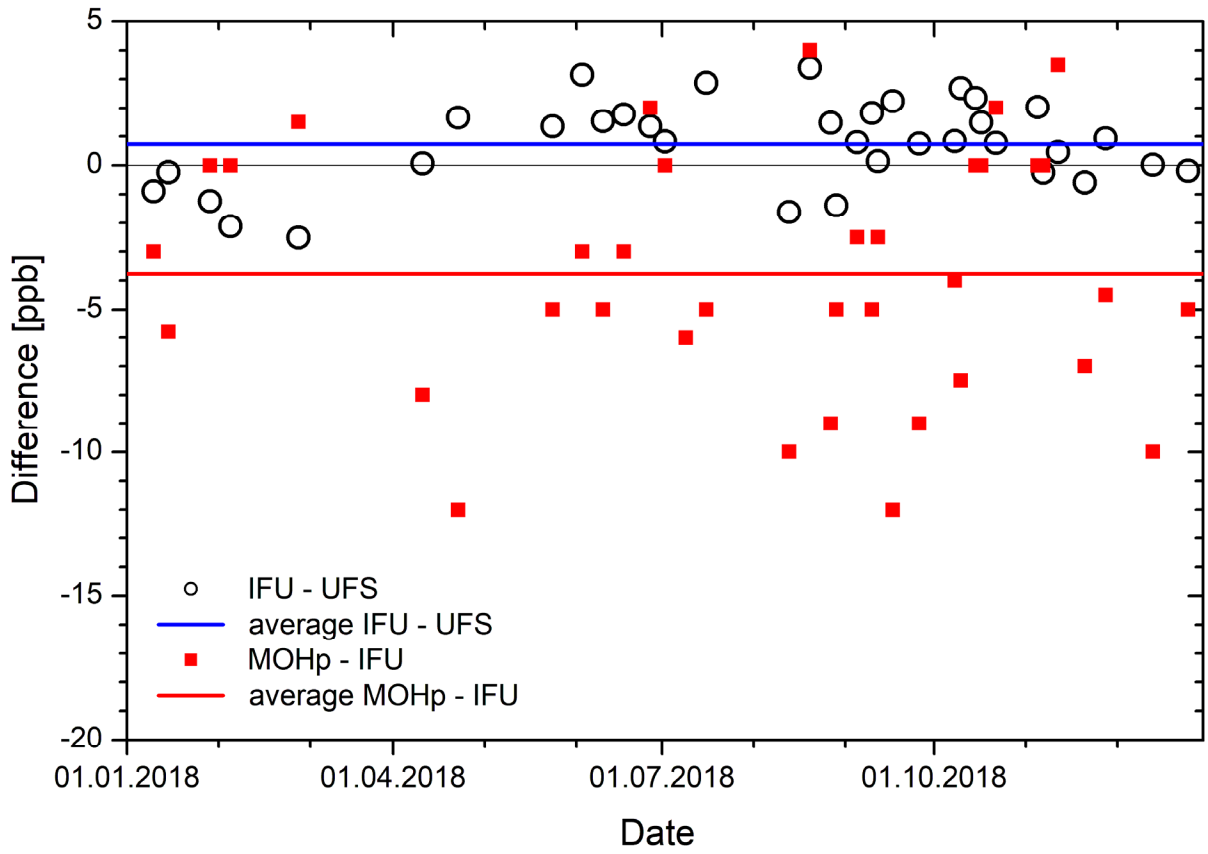
Fig. 10. Differences between the ozone values of the IFU DIAL at 2670 m and the UFS routine measurements as
well as the offsets of the MOHp profiles with respect to the DIAL for 35 of the 36 measurement days of the 2018
comparison. The blue and red horizontal lines are the arithmetic averages for the full year (for the values see
text).
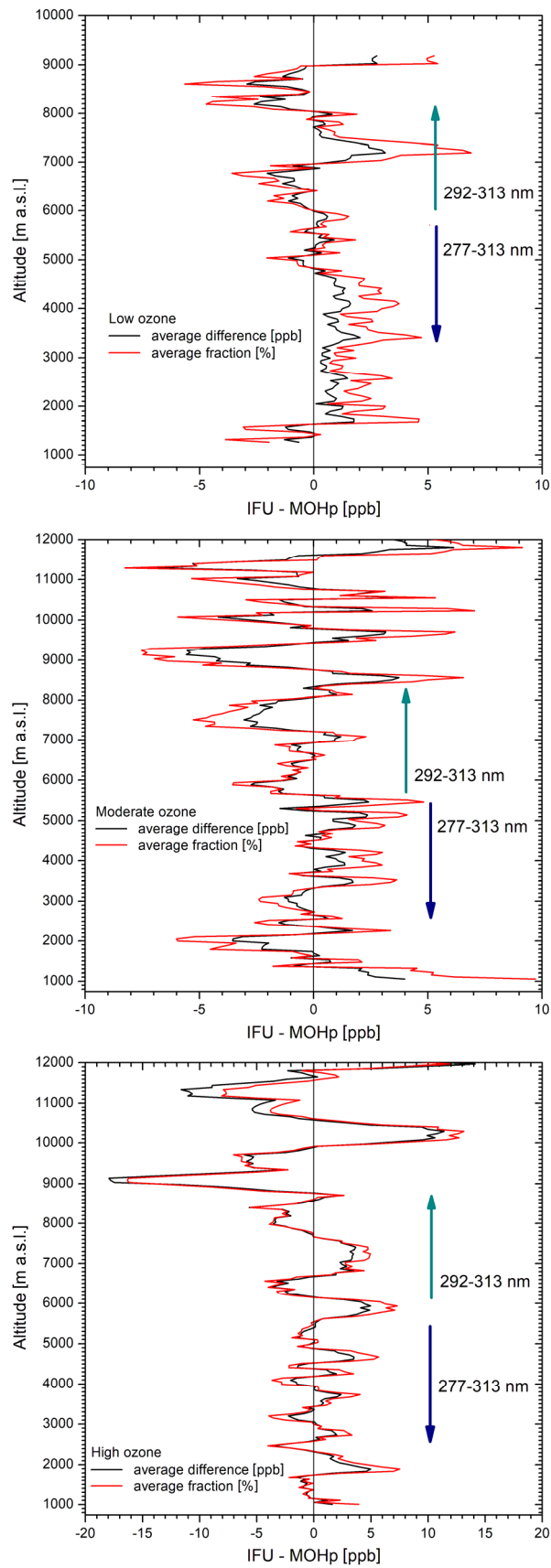
Fig. 11. Average differences between IFU lidar and offset-corrected MOHp sonde in 2018 for low-, moderate and high-conditions (based on six, seven and six comparisons, respectively); the uncertainties may be estimated from the maximum differences around the respective altitudes. We also indicate the approximate altitude ranges of the two wavelength pairs used for the lidar data evaluation.

973
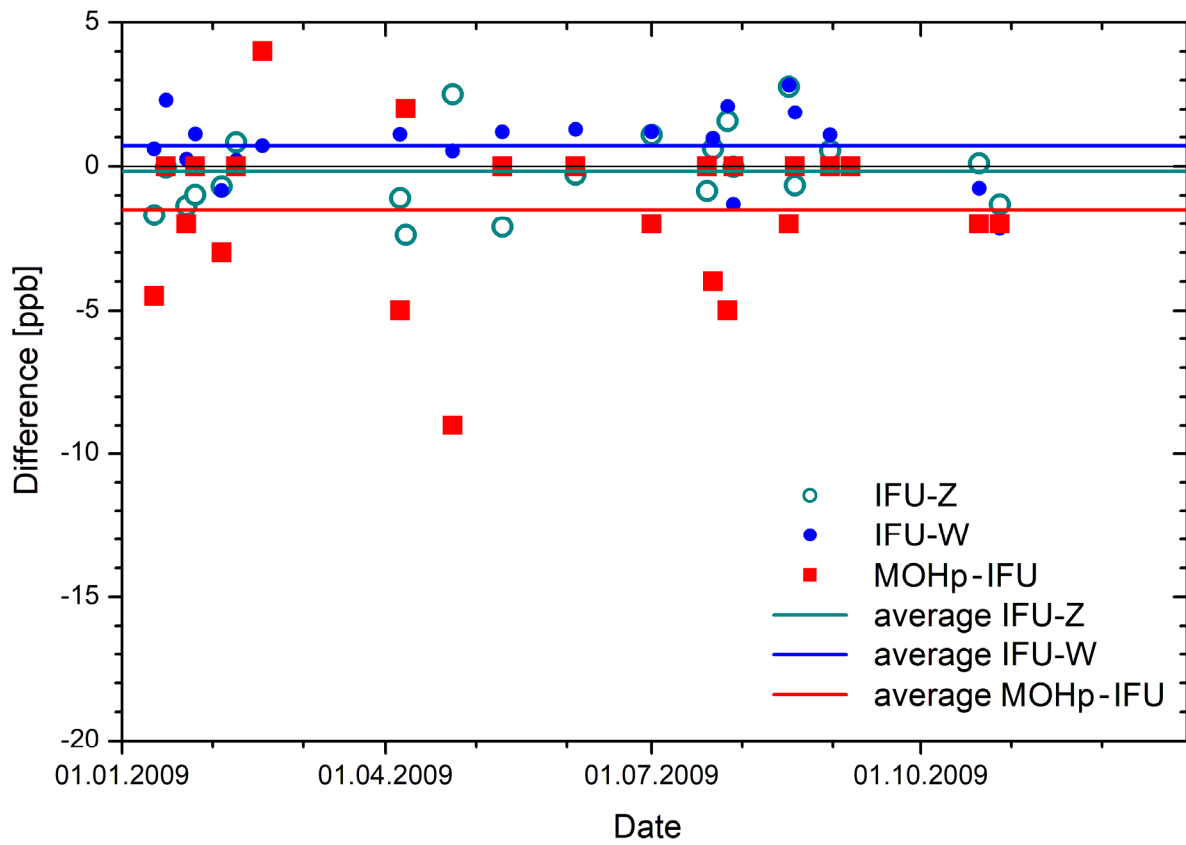
974 **Fig. 12**. Differences between the ozone mixing ratios of the lidar (IFU) and the stations Zugspitze (Z), Wank
975 (W) at the summit altitudes, and offsets between lidar and MOHp sonde for 2009
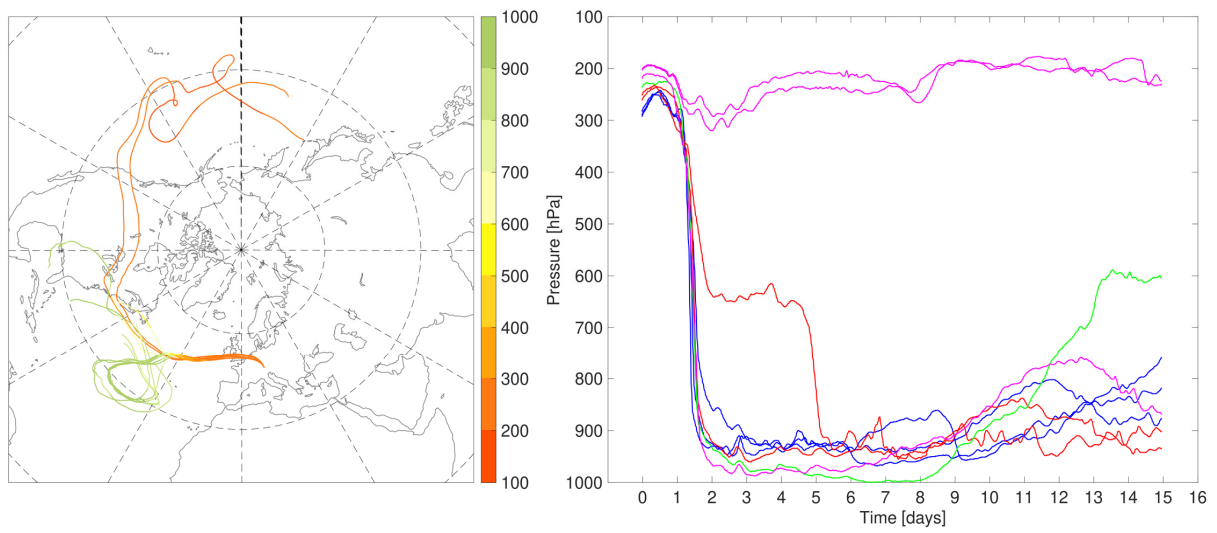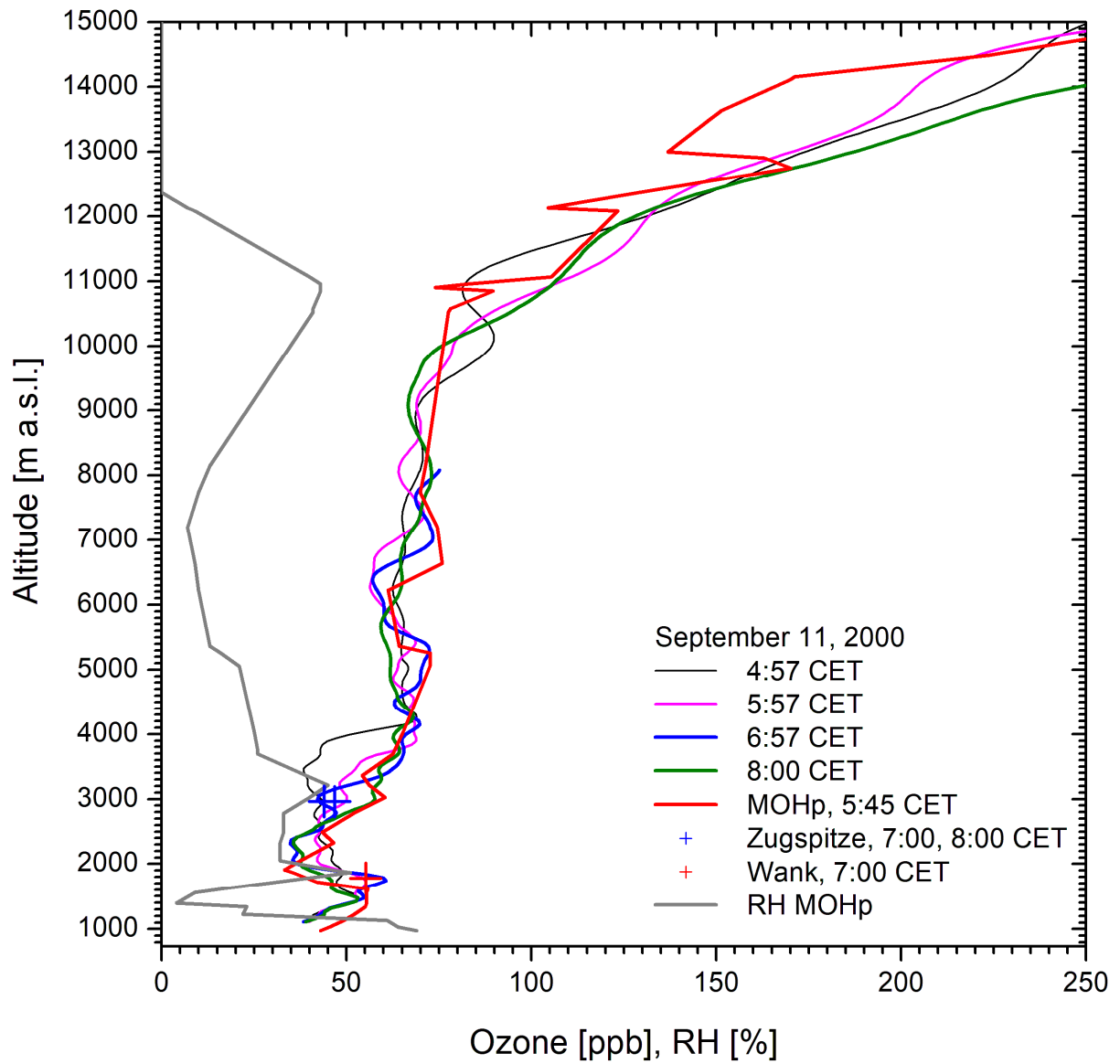976
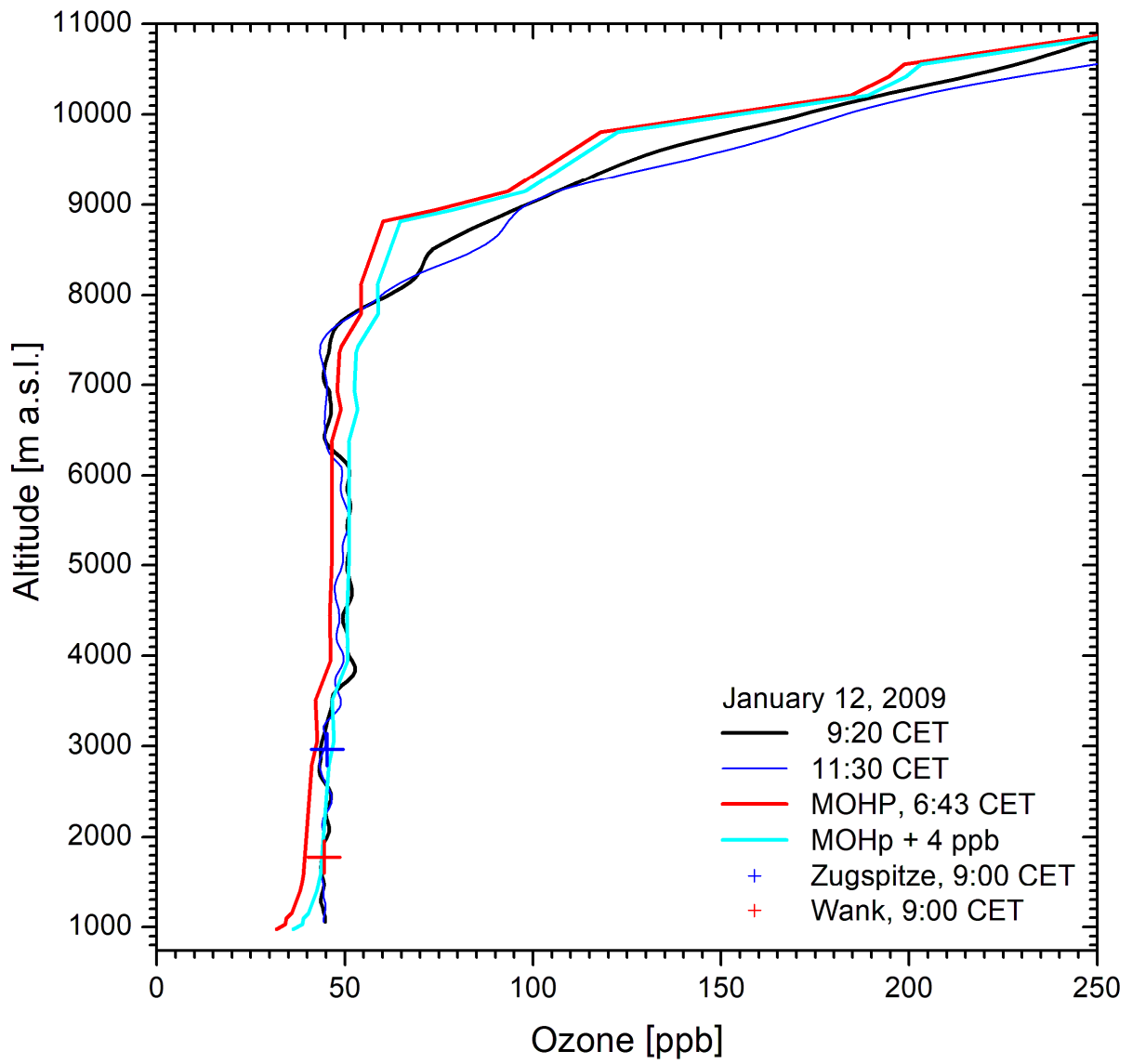
Fig. 13. Ozone measurements on 12 January 2009
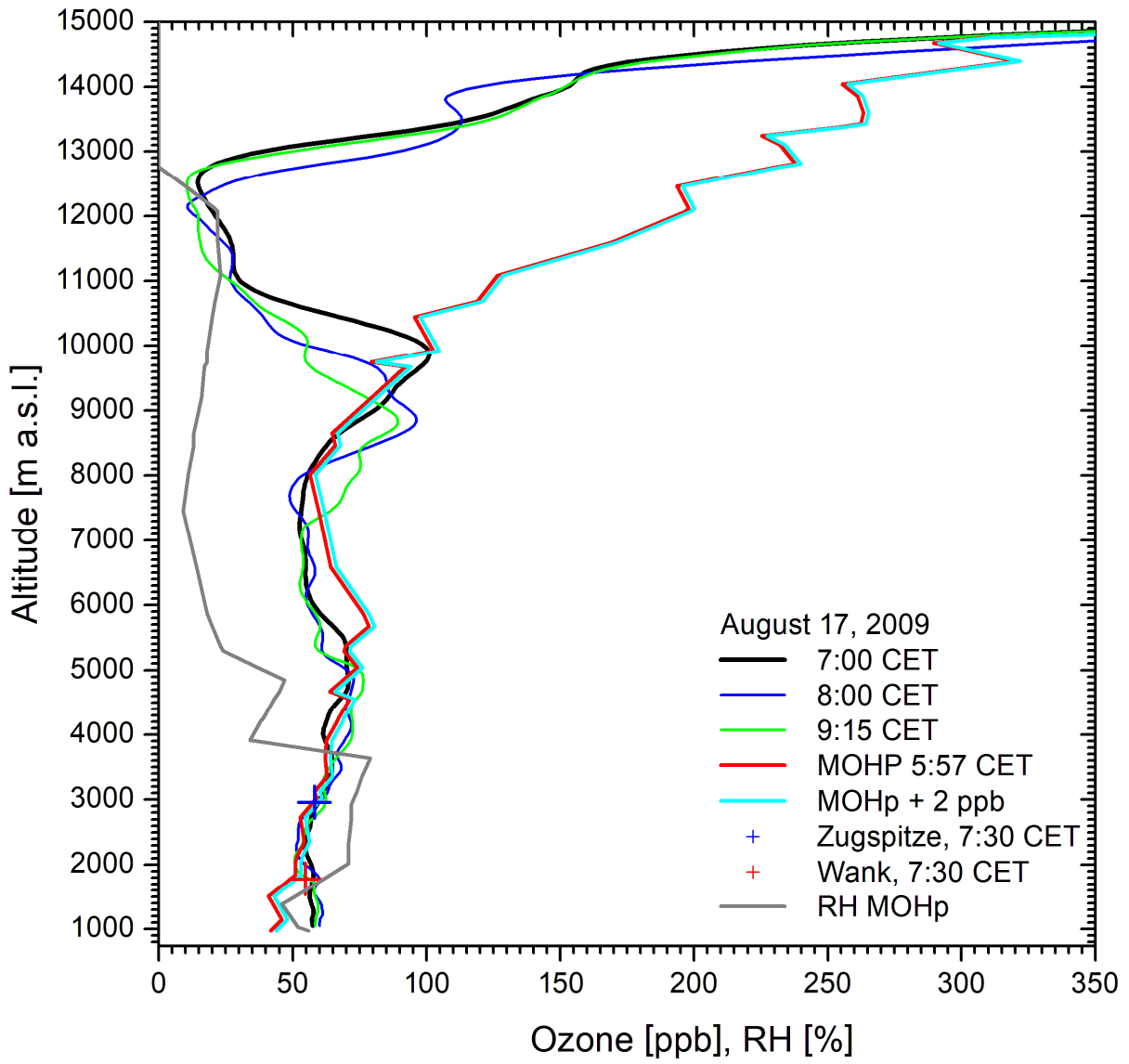
Fig. 14. Ozone measurements on 17 August 2009; the structure in the upper troposphere is strongly influenced
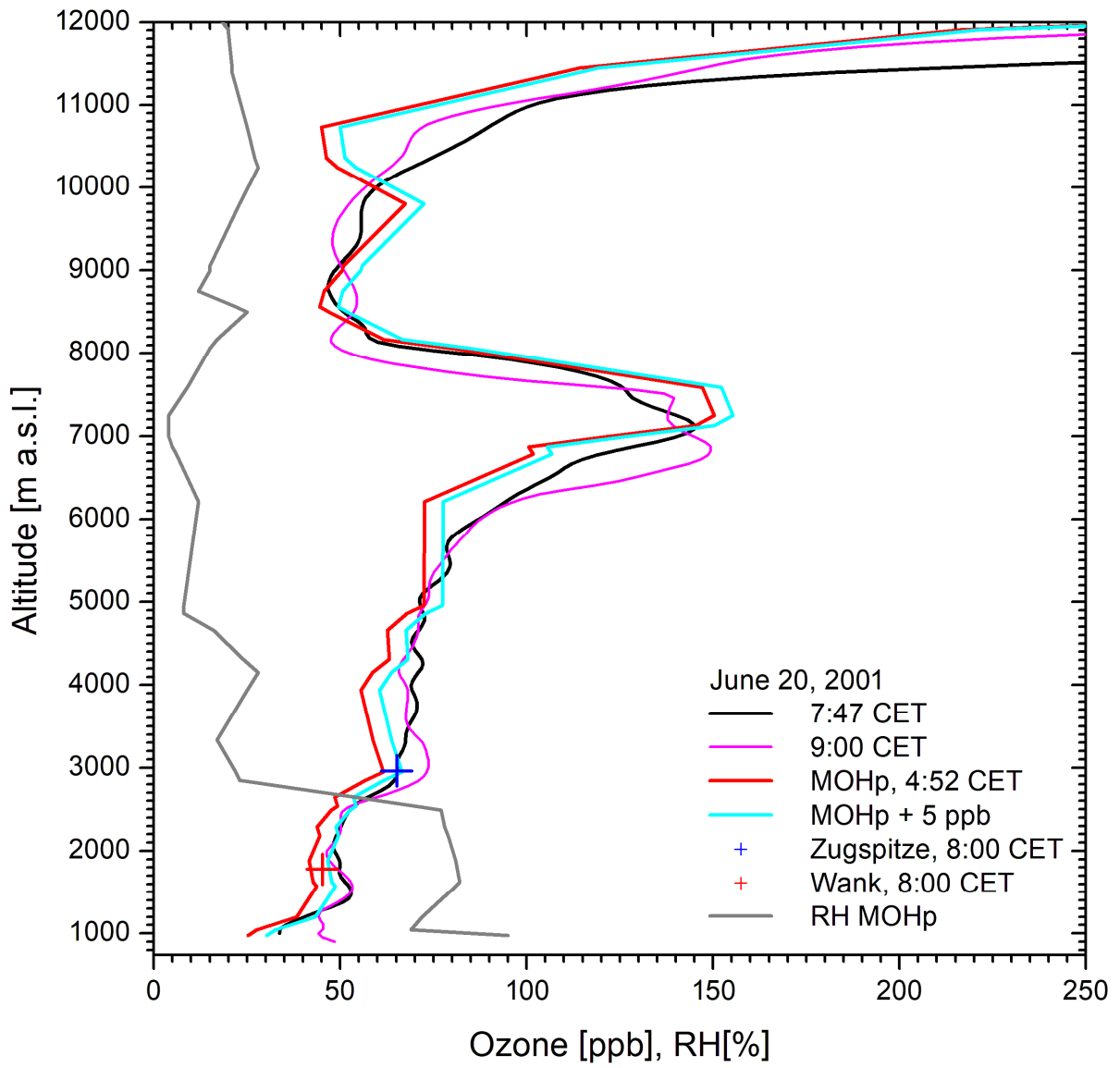by smoothing. The bias between 5.5 and 8 km has not been explained.

984

985   **Fig. 15.** 350-h LAGRANTO backward trajectories, started above Garmisch-Partenkirchen (G) on 9 July 2018 at
986   7:00 CET
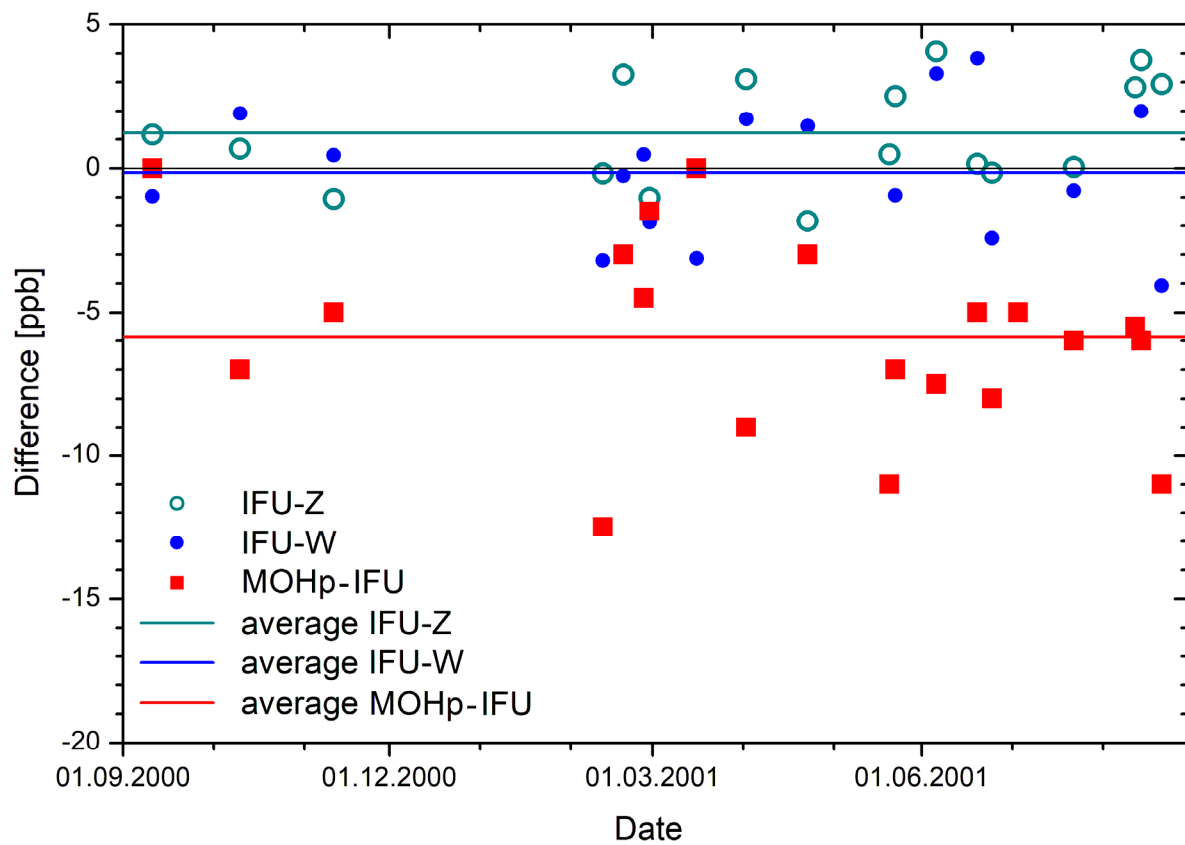
987

Fig. 16. Ozone measurements on 11 September 2000 (see Fig. 13 of Trickl et al., 2003); in this case no offset
was determined.

Fig. 17. Ozone measurements on 20 June, 2001; the entire temporal development of the stratospheric air
intrusion around 7.3 km is depicted in Fig. 6 of Zanis et al., 2003, and Fig. 3 of Trickl et al., 2010)

996

997   **Fig. 18.** Differences between the ozone mixing ratios of the lidar (IFU) and the stations Zugspitze (Z), Wank
998   (W) at the summit altitudes, and between lidar and MOHp sonde, determined by shifting the sonde profile, for
999   the period September 2000 to August 2001.